Optical study of rare earth ion and transition metal impurities in nitrides

Von der Fakultät für Elektrotechnik, Informationstechnik, Physik
der Technischen Universität Carolo-Wilhelmina
zu Braunschweig
zur Erlangung des Grades eines
Doktors der Naturwissenschaften
(Dr.rer.nat.)
genehmigte
D i s s e r t a t i o n

von Jayanta Kumar Mishra
geboren in India (Saharpada, odisha)

1. Referee: Prof. Dr. A. Hangleiter
2. Referee: Prof. Dr. S. Kück

eingereicht am: 15. 07. 2013

mündliche Prüfung (Disputation) am: 09. 09. 2013

Druckjahr: 2013

Prior publications of the dissertation

Partial results from this work were published with the permission of the Faculty of Electrical Engineering, Information Technology, Physics, represented by the supervisor of the thesis in the following articles:

Publication:

J. K. Mishra, T. Langer, U. Rossow, S. Shvarkov, A. Wieck, and A. Hangleiter, *Strong enhancement of Eu+3 luminescence in europium-implanted GaN by Si and Mg codoping*, Applied physics letter, **102**, 061115, 2013.

Conferences:

- J.K. Mishra, T. Langer, K. Trunov, R. Schott, U. Rossow, A. Wieck, and A. Hangleiter, *Optical studies of europium in GaN*, IGSM summer school Goslar 2008.
- J.K. Mishra, T. Langer, K. Trunov, R. Schott , U. Rossow, A. Wieck, and A. Hangleiter, *Optical study of rare earth ion implantation in GaN heterostructures*, DPG Meeting, Dresden 2009.
- J.K. Mishra, T. Langer, K. Trunov, R. Schott ,U. Rossow, A. Wieck, and A. Hangleiter, *Effect of Mg codoping on Europium(Eu^3+) implanted GaN* DPG Meeting, Regensburg, 2010.

- J.K. Mishra, T. Langer, K. Trunov, U. Rossow, A. Wieck, and A. Hangleiter, *Europium implanted AlGaN: A promising system for controlled photon emission*, International Workshop on Nitrides , Florida, USA 2010.

- J.K. Mishra, T. Langer, K. Trunov, U. Rossow, A. Wieck, and A. Hangleiter, *Optical studies of europium in p-GaN* , IGSM summer school Burg Warberg, 2010.

- J.K. Mishra, T. Langer, K. Trunov, U. Rossow, A. Wieck, and A. Hangleiter, Eu^3+ *luminescence in III-Nitrides by alloying and co doping*, E-MRS fall Meeting, Warsaw, Poland 2011.

- J.K. Mishra, T. Langer, K. Trunov, U. Rossow, A. Wieck, and A. Hangleiter, *Optical studies of Europium(Eu+3) implanted of Mg codoping on GaN*, DPG Meeting, Dresden 2011.

- J.K. Mishra, T. Langer, K. Trunov, U. Rossow, A. Wieck, and A. Hangleiter, *Identification of different sites in europium implanted Mg doped GaN*, IGSM summer school, Burg Warberg 2012.

- J. K . Mishra, T. Langer, K. Trunov, U. Rossow, A. Wieck, and A. Hangleiter, *Study of europium site symmetry from europium-implanted p-GaN*, DPG Meeting, Berlin 2012.

Abstract

Europium (Eu) and other rare earth ions along with some transition metals doped in nitride semiconductor has been investigated by photoluminescence measurement. Eu has been found to be most efficient light emitting dopants. Eu was implanted on several host materials (undoped GaN, Mg-doped GaN, u-AlGaN, Mg-doped AlGaN, AlN). We propose a new method to distinguish optically active centers of Eu in Eu-implanted Mg-doped GaN. Two different types of optically active Eu centers in Mg-doped GaN:Eu and one types of centers in undoped GaN:Eu has been identified. Sevral more optical centers in Mg-doped GaN:Eu can not be ruled out. The excitation mechanism of these Eu centers based on rate equations was formulated by a donor-acceptor pair (DAP) resonant energy transfer model where europium ions are excited by those donor-acceptor pairs located from a certain distance to match one of its excited energy level with the DAP transition energy. For above band gap excitation the formation of randomly distributed indistinguishable neutral donors and acceptors around the europium ions dominates the characteristics of the energy transfer process. From the temperature-dependent photoluminescence measurements by above band gap excitation two activation energies (106 meV and 0.6 meV) for one type of Eu center is derived. Under below band gap excitation no nonradiative energy back transfer has been observed at higher temperatures as the luminescence efficiency remains constant. Surpris-

ingly the PL lifetime of Eu^{3+} spectra is found to be approximately the nearly same at all temperatures, which further confirms the radiative emission. Europium ion is supposed to be excited by a resonant energy transfer from the donor-acceptor pair in the vicinity of the europium ions which are directly excited by the optical excitation.

A strong enhancement of Eu^{3+} luminescence in europium-implanted GaN samples is obtained by codoping with silicon (Si) and magnesium (Mg) simultaneously. The Eu^{3+} intensity in the $^5D_0$ to $^7F_2$ transition region is found to be thirty times higher compared to europium-implanted undoped GaN. The major contribution to this overall enhancement is due a weak peak present only in europium-implanted Mg-doped GaN at 2.0031 eV (618.9 nm) which is strongly enhanced by codoping both Mg and Si. The excitation process of europium ions is considered to take place through a donor-acceptor pair related energy transfer mechanism.

Moreover, the Eu^{3+} luminescence even higher in AlGaN materials. Eu^{3+} luminescence has been studied in different Al composition with different doping (Mg and Si). The peaks position in GaN to AlN has been found to be red shifted as a consequence of change in crystal field.

Contents

List of Figures

1 Introduction

Optoelectronic devices are becoming vital part of everyday life. Earlier fluorescence based light sources were used to serve this purposes. Laser diodes (LDs) and light emitting diodes (LEDs) are commonly used in fiber optical communications, traffic signals and in many such applications. Nitride semiconductor has been widely studied recently for the opto electronics devices basically for light emitting diodes and lasers structures.

Rare earth ions in semiconductors have been widely discussed for possible applications in optoelectronic devices [1],[2] They show very sharp luminescence lines which hardly depend on temperature and crystal host. Eu^{3+} emits light as the electrons in its 4f orbital undergo transitions from higher excited states to the ground state. Europium and Erbium are considered to be most useful among rare earth ions because they emit light in the red and green region of the visible spectrum. In particular, Europium in GaN is being studied because of its potential to extend the spectrum of nitride-based light emitters into the red region [3],[4].

In situ doped GaN:Eu grown by MOCVD or MBE has been investigated [1][5]. Recently Nishikawa et al. reported current injected red emission from p-type/ Eu-doped / n-type GaN: Eu red LED with optical output power of 1.3 μW at 620 nm [2]. The same group also reported a higher optical power of 17 μW using atmospheric pressure MOVPE [6].

However higher luminescence efficiency is still a need for fabricating efficient commercial optical devices. One way to enhance Eu^{3+} luminescence intensity in GaN is codoping by Mg as the transition probability depends on crystal symmetry [7],[8]. Si doped GaN grown by MBE has shown 5-10 fold higher Eu^{3+} luminescence intensity compared to undoped GaN:Eu[9]. Wang et al. claimed that the Si codoping might increase the excitation cross-section and an efficient energy transfer by shallow energy levels. Er-implanted Mg doped GaN was investigated and also exhibited selective enhancement [8] of Er^{3+} luminescence intensity. Recently, europium doped GaN with Mg co doping grown by ammonia MBE has also been reported [10]. Enhanced Eu^{3+} luminescence has been observed intensity by Mg codoping in *in situ* europium doped GaN.

Along with higher luminescence by codoping, Eu^{3+} emission spectra have contributions from multiple optical centers [11],[12]. Tagaki et al.[10] mentioned those sites as A and B and relative concentration of those centers were calculated. We assigned similar centers as type I, type II and so on.

The energy transfer process from GaN to Eu^{3+} is a complicated process. Several authors have explained the excitation process of Eu^{3+} in different hosts. Some assumes that the energy transfer takes place through a charge transfer state [13],[14]. But there is no complete model in previous literature available for energy transfer mechanism from GaN to europium ion. An energy transfer process through the donor-acceptor pairs has been proposed..

The goal of this work was to fabricate single photon sources using the nitride semiconductor. We have used several RE ions and transition metals to implant on nitrides host for this purpose. Europium found to be the only material which can emit light from the nitride hosts. However, the luminescence lifetime was found to be very large for an efficient single

photon source. Other rare earth ions and transition metals does not show any significant luminescence. Therefore, we mostly studied the europium luminescence.

In the first chapter, GaN and other rare earth ion and transition metals properties are described. In second chapter spectroscopy of europium in different host is discussed. In the third chapter, the experimental set up is described, in the fourth chapter the experimental results have been explained by the proposed model. In fifth chapter all the works are concluded and summerized.

2 Basic properties of investigated materials

2.1 Gallium Nitride and its alloys

GaN and its alloys are very promising in fabricating optoelectronic devices. The extensive bandgap engineering can be possible with these III-V semiconductors. For example the alluminium nitride (AlN), gallium nitride (GaN) and indium nitride (InN) have a bandgap of 6.1 eV, 3.4 eV and 0.7 eV [15, 16, 17] respectively at room temperature. So in principle nitride semiconductors could be used for light emission in the wavelength range between IR(1.5 μm) to ultra violet region (200 nm). However, it is difficult to produce nitride based lasers at higher wavelengths. The efficiency decreases substantially when lasers or LEDs operating in the long wavelength region above 500 nm due to the necessity of incorporating high indium contents. This induce strain related defects in the lattice. Additionally, The piezo fields created due to the strain lead to low overlap between the electron and hole wave functions which is the reason for low efficiency [18, 19]. GaN is the primary material among the nitride semiconductors. It can exist at least in two types of crystal structures, cubic and hexagonal (wurzite). The unit cell of wurzite crystal structure is shown in figure 2.1. It has two lattice constants represented as a and c with space group of $C_{6v}^4 - P6_3$mc. The value of a-lattice constant and c-lattice constants at room temperature are 3.186 $\overset{\circ}{\text{A}}$ and 5.186 $\overset{\circ}{\text{A}}$

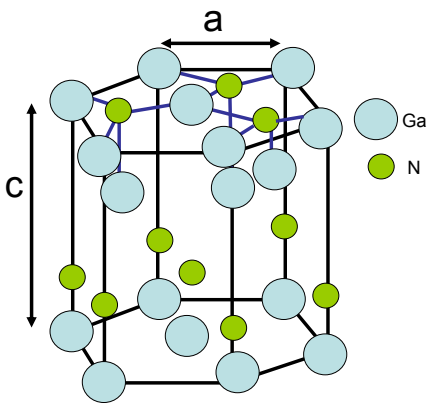

Figure 2.1: Schematics of GaN unit cell.

respectively. In addition to that GaN is significantly ionic and partially covalent bonded among the gallium and nitrogen atoms.

The unit cell of GaN in wurzite structure consists of 2 Ga and 2 N atoms with a density of 6.15 g/cm^3. Experimentally GaN thin films can be grown on various substrates. The lattice mismatch between the substrate and the grown layer can be calculated as follows

$$\frac{a_{layer} - a_{substrate}}{a_{substrate}}$$

where a_{layer} is the lattice constant of the grown layer, $a_{substrate}$ is lattice constant of the substrate. Large lattice mismatch between substrate and the layer leads to poor crystalline quality of the layer. In order to reduce the lattice mismatch, a low temperature nucleation layer following a buffer layer are usually grown on the substrate. Sapphire and 6H or 4H SiC are the the mostly used substrates. However, Sapphire is transparent and cheaper compared

to SiC.

2.2 Rare earth (RE) ions

Rare earth ions are not rare in the earth crust. They are typically dispersed and not found in concentrated form. That is the reason why they are named rare earth. The free ion energy levels of all rare earth ions are in figure 2.2. During the work we have used three different RE ions: cerium, europium and erbium

2.2.1 Cerium

Cerium (Ce) is the 1st element in the lanthanide series in the periodic table, it has an atomic number of 58 and the electronic configuration is [Xe] 4f 5d $6s^2$. It can exist in 3+ charge state in various solids. Usually most transitions in cerium are parity allowed unlike other rare earth ions such as europium and erbium. This is because the transitions involved are not in the same orbital rather than in different orbitals (5d to 4f), so allowed by parity. For example at 560 nm a broad line is observed in Ce doped yttrium aluminum garnet [20]. Cerium doped GaN has been studied as well [21]. But no luminescence which corresponds to cerium is observed except only a shift in the band edge luminescence of GaN. The interaction between of the electrons in the 5d orbital and the host material results in a broadening of the spectrum [22]. It is found that cerium-doped yttrium aluminum garnet YAG:Ce is the most suitable yellow luminescent phosphor for the production of white LEDs [23, 24]. The lifetime of Ce luminescence are comparably very short, typically in the order of ten nanoseconds. Hansel et al. [25] showed the luminescence lifetime of cerium-doped yttrium aluminum garnet as a function of temperature and as a function of gallium content.

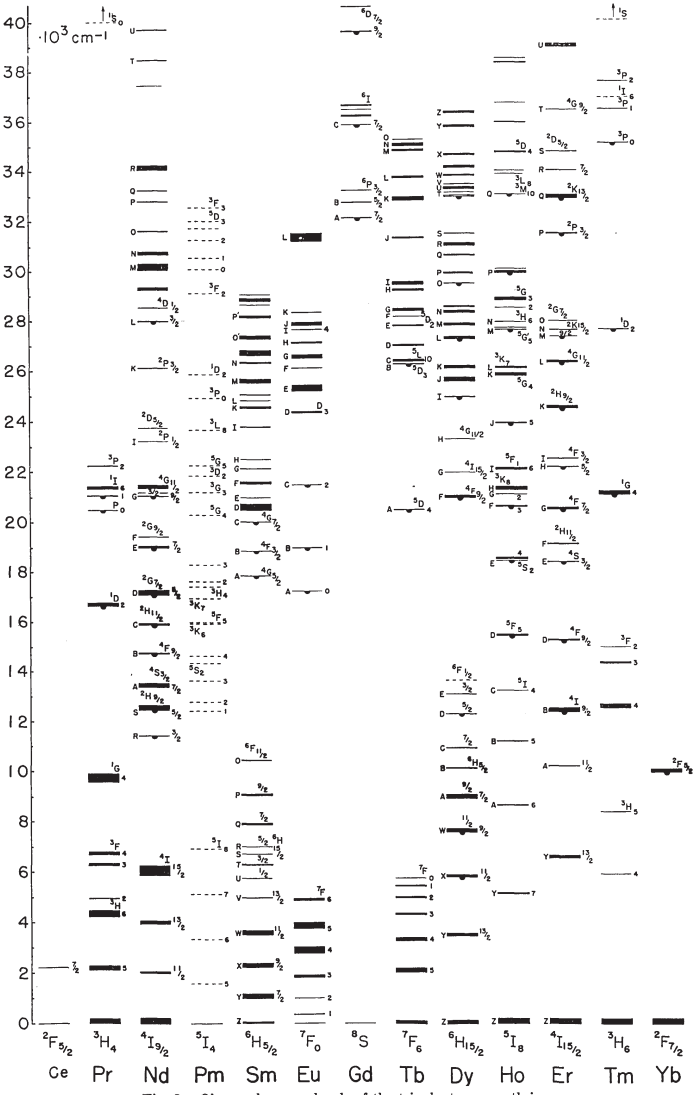

Figure 2.2: Free energy level of rare earth ions (Applied Optics, OSA, 2, 675-686 (1963))[26]

They found a further decreasing of decay lifetime with increasing gallium content. Shorter lifetime was a concern of study for the efficient single photon devices.

2.2.2 Europium

Europium (Eu) is the sixth element of the lanthanide series in the periodic table. The electronic configuration of Eu is $[Xe]4f^7 5p^6 6s^2$. It has two possible charge states +3 and +2 in various solid hosts. The charge state basically depends on the host material. The electronic configuration of Eu^{3+} is $[Xe]4f^6 5p^6$. For different charge states the emission wavelength changes in Eu doped material. For +2 charge state it emits a broad line at 460 nm [27] as the transitions are dipole allowed. Luminescence from Eu^{2+} has been extensively studied as phosphor material to fabricate white LEDs. In various phosphor materials such as alkaline-earth-metal halophosphates are well known for their applications in optical devices. Among these, divalent europium-activated strontium chlorophosphate is an efficient photoluminescent material, used as the blue component in high efficiency compact fluorescent lamp. Eu^{2+} doped barium chlorophosphate ($Ba_5(PO_4)_3Cl$: Eu^{2+}) is a promising material for X-ray imaging [28]. White light-emitting diodes (LEDs) using Eu^{2+} phosphor offer reliability, energy saving, and safety [29].

However, for +3 charge state it has an intense sharp emission line in between 610 to 620 nm according to the solid hosts. This is an electronic transition from the energy level $^5D_0$ to $^7F_2$. This transition energy is independent of temperature in a particular host and varies only slightly from host to host. Because the electrons involved in such transitions are interacting very weakly with the host atoms. The emission intensity and excitation efficiency depend on the host material.

Due to the crystal field energy levels of rare earth ions are split into several sub levels. The Eu^{3+} luminescence is particularly useful in studying local environment as it possesses non-degenerate ground ($^7F_0$) and emitting ($^5D_0$) states, so that neither the ground nor emissive level can be split by a crystal field. Thus a one-to-one correspondence exists between the number of peaks ($^5D_0$ to $^7F_0$) in the emission spectrum and the number of distinct Eu^{3+} ion environments [30]. In different solid hosts Eu^{3+} occupies different site symmetries, for example in calcium tartrate tetrahydrate material Eu^{3+} occupies a D2 symmetry [30] whereas in Y_2O_3 it occupies a C2 symmetry [31]. In addition to that Eu^{3+} expected to occupy a C_{3v} symmetry site in GaN [32].

2.2.3 Erbium

Erbium (Er) has the electronic configuration [Xe] $4f^{12}$ $6s^2$. It exists in 3+ charge state in most of the solid materials. Er basically emits in the green region (532 nm) of the visible spectrum and in the infrared region (1.5 μm). The infrared emission is due to the electronic transition from the excited energy level $^4I_{\frac{13}{2}}$ to the ground state $^4I_{\frac{15}{2}}$ and for the visible range emission due to the electronic transition of $^4I_{\frac{15}{2}}$ to $^2H_{\frac{11}{2}}$ [33, 34]. The infrared (1.5μm) emission is very suitable for optical fiber communication due to minimum loss for this wavelength. For this purpose it is essential to know about its emission properties. LEDs based on Er doped silicon is being fabricated [33]. Moreover, an Erbium-doped microlaser is fabricated utilizing SiO_2 microdisk resonators on a silicon chip [35].

Er in silicon is well investigated due to its possible application in microphotonic technology. The excitation mechanism is discussed by an Auger kind of recombination. The recombination processes of Er in silicon are different because of the localized nature of core f-electrons. Palm et al. [36] derive the radiative and nonradiative mechanisms of the

energy transfer in erbium doped silicon by investigating the temperature dependence of the intensity and the photoluminescence lifetime. They have found that the nonradiative energy back transfer from the excited Er ion to the Si host causes luminescence quenching which is a impurity Auger effect. This is certainly an efficient luminescence quenching mechanism for Er luminescence in Si. They proposed an excitation mechanism in which rare earth ions are excited by excitons and a decrease of radiative efficiency by Auger back energy transfer from the rareearth ions to the free electrons. A similar conclusion is also observed by Thao et al. [37].

2.3 Transition metals

The transition metals are the elements in the d-block of the periodic table. There is a common feature between the transition metals and rare earth metals. Unlike rare earth metals, transition metals have also partial occupancy in d- orbital. Following are the materials we studied.

2.3.1 Chromium

Chromium (Cr) has the electronic configuration [Ar] $4s^1 3d^5$. Cr has a typical electronic transition from E_2 to $^4A_2$ which gives rise to two emission lines called R1 and R2 at 694 nm and 692.5 nm [38]. Cr can be present as an impurity in sapphire [39]. If sapphire has more than 1000 ppm Cr^{3+} ions as impurities, it is referred to as a ruby. In case of ruby, the optical processes result from the electronic transitions at the outer $3d^3$ shells of the Cr^{3+} ions. The unshielded character of these orbitals, makes Cr^{3+}-related light emission very efficient. The Cr^{3+}-related luminescence are highly affected by the crystal environment. These are used in solid-state lasers such as ruby laser which produces light emission at 694

nm [40]. The Cr^{3+} ion is slightly larger than Al^{3+} and normally substituting the aluminum in sapphire. The first optical laser achieved by stimulated optical emission from a solid-state device based on ruby or Cr^{3+}-doped sapphire [41].

The Cr^{3+} ion is also found to be doped in AlN in different substrates such as silicon and optical fibers [42]. Strong light emission occurred at 702 nm, which is a sharp peak that corresponds to a transition from $^4T_2$ to $^4A_2$ of Cr^{3+} ion. A number of other optical and photonic device can be constructed using this strong emission from AlN:Cr.

2.3.2 Cobalt

Cobalt (Co) has electronic configuration [Ar] $4s^2$ $3d^7$. Cobalt doped materials are basically known for their magnetic properties [43]. Due to their spin-transport properties, the transition-metal doped semiconductors are referred as diluted magnetic semiconductors and there is a possibility of its application in spintronic devices. The unique electronic structure of Co induces the room temperature ferromagnetism [44]. Simultaneously semiconducting and ferromagnetic behavior is observed in Co-doped TiO_2 above the room temperature [45] as well.

In addition, Co doped ZnO shows optical properties and it exists in +2 charge state. The emission line at 662 nm can be interpreted as an electronic transition from $^2E(^2G)$ to $^4A_2(^4F)$ in the Co^{2+} ions under the tetrahedral crystal field (T_d) imposed by the host material, ZnO [44].

2.3.3 Nickel

Nickel (Ni) has electronic configuration [Ar] $4s^2$ $3d^8$. Like cobalt doped material Ni also acts as a magnetic semiconductor when doped into semiconductor host material. For exam-

ple Ni doped ZnO shows room temperature ferromagnetism [46]. Paramagnetic behavior in nickel doped ZnO has also been observed [47]. Nickel exists in 2+ charge state in most of the host materials. Moreover, Nickel doped material shows luminescence properties as well. The room-temperature photoluminescence of CdS:Ni nanoparticles was observed at 503 nm. This emission of CdS:Ni is attributed to the $^1T_{2g}$(D) to $^3A_{2g}$(F) electronic transition of 3d orbital. The intensity of this transition increases with an increase of the Ni^{2+} concentration [48].

2.4 Co-doping in GaN

2.4.1 Magnesium-doped GaN

Magnesium (Mg) is a well known acceptor in GaN. The typical photoluminescence (PL) spectrum in Mg-doped GaN is a blue luminescence (BL) band with a maximum at about 2.8 - 2.9 eV (420 - 450 nm) [49]. This BL band is a typical emission from donor acceptor pair luminescence (DAP). The peak position of emission spectra from Mg-doped GaN depend on Mg concentration as well. Apart from the luminescence from a dislocation center at 3.01 eV, there exists a photoluminescence band near 3.28 eV (378 nm) at lower Mg-doping level. This band is due to the transition from a shallow donor, a possible candidate is gallium vacancy (V_{Ga}) to an acceptor which is possibly an isolated substitutional Mg (Mg_{Ga}). The binding energy of the acceptor was found to be in the range of 200 meV to 250 meV [49, 50, 51, 52]. However at high Mg concentrations, a photoluminescence center at 2.8 - 2.9 eV has been observed which is attributed to a deep donor and acceptor pair transition. This deep donor consists of a defect structure of Mg_{Ga} - nitrogen vacancy (V_N) complex and the acceptor is an isolated Mg_{Ga} [50, 51, 52, 53]. The deep Mg-related donors (Mg_{Ga}

–V_N complex) were found to be at 500 meV below the conduction band which is responsible for the 2.7-2.8 eV emission [52]. From the temperature dependent photoluminescence study, it is found that the intensity of the blue emission (2.7-2.8 eV) decreases gradually as temperature increases which is attributed to the quenching phenomena of the DAP emission. This quenching phenomena is due to thermal activation with a Mg acceptor energy of approximately 160 meV [51]. Mg doping induces potential fluctuations in the band edges in Mg-doped GaN which results a quadratic dependence of the PL intensity on the excitation power density. The donor acceptor pairs are generally spatially separated to each other and attracted by coulomb interaction. The recombination energy is given by the following formula [51]

$$h\upsilon = E_g - (E_D + E_A) + \left(\frac{e^2}{\varepsilon r}\right)$$

where E_g is the band gap, E_D and E_A are the donor level with respect to conduction band and acceptor level with respect to valence band respectively and r is the average distance between the donor and acceptor. The last term represents the coulomb interaction between spatially separated donors and acceptors.

The concentration of holes increases with increasing Mg doping level but after a certain Mg concentration, it begins to decrease. The hole concentration has been measured by Hall measurement [53]. This reduction in the hole density is due to the compensation of the Mg species by Mg-related defects introduced at high Mg doping. This defect could be a complex formed by nitrogen vacancy and Mg.

Mg doping enhances the rare earth luninescence efficiency in GaN. It has been observed that the Er luminescence in Er-implanted Mg-doped GaN is selectively enhanced compared

to in Er-implanted undoped GaN [54]. In the Er-implanted Mg-doped GaN, the 1.5 μm erbium characteristic luminescence are significantly enhanced by Mg doping. This Er center is excited by a 2.8-3.4 eV below-gap photoluminescence excitation (PLE) band. Erbium luminescence dominates the above-gap excited PL spectrum of Er-implanted Mg-doped GaN, in contrast it disappears in Er-implanted undoped GaN.

Mg doping in GaN enhances the Eu luminescence in europium-doped GaN as well[7, 10]. Lee et al. observed five times higher luminescence in Mg co- doping in GaN. The Mg related peaks show highest luminescence at 180 K [7] at the same time the PL lifetime decreases towards room temperature. The effect of Mg co-doping also investigated by Tagaki *et al.* [10]. They have observed a 20-fold enhancement of Eu^{3+} luminescence after Mg co-doping. Mg could selectively activate the Eu optical site by elimination of nonradiative deexcitation paths from the excited state $^5D_0$.

2.4.2 Silicon-doped GaN

Silicon (Si) is a well known donor in GaN [55]. The near band edge emission is quite prominent in Si doped GaN. In addition to that, there is a weak transition centered at 2.2 eV which is commonly known as the yellow luminescence band [56, 57]. The origin of this emission is well described by a recombination model involving shallow donors and deep defects. This emission is generally expressed as following equation similar to the blue band in p-GaN [51].

$$h\nu = E_g - E_D - E_A + \frac{e^2}{\varepsilon r}$$

Here E_g is the band gap, E_D and E_A is the donor and acceptor levels respectively and r is the average distance between the donor and acceptor. The last term represents the coulomb

interaction between spatially separated donor and acceptor. The intrinsic defects can act as donors and introduce deep levels in the bandgap.

Si codoping in GaN is also found to enhance the RE luminescence in GaN [9]. Eu and Si codoped GaN thin films were investigated. Eu^{3+} photoluminescence emission at 622 nm was enhanced by approximately five to ten times with Si doping. Different Si codoping affected the PL intensity and lifetime. Moderate Si doping lead to an increase in Eu^{3+} lifetime and enhanced PL intensity whereas high Si doping significantly quenches the PL intensity and lifetime due to nonradiative channels produced by a high defect concentration.

3 Selection rules and Excitation process

3.1 Brief selection rules for single electron case

As hydrogen atom is a single electron atom, selection rules for optical transitions can easily be derived [58]. If the electronic states are represented by the principal quantum number n and the orbital quantum number l, m and spin quantum number as s according to Laporte selection rule for a transition the difference in principal quantum number between the quantum levels should be $\Delta n = 0, \pm 1, \pm 2, \pm 3...$ and so on however, the change in orbital quantum number should be $\Delta l = \pm 1$, $\Delta m = 0, \pm 1$ [58].

The spectroscopic transitions between the states depend on whether the transition from the initial state i to the final state f is allowed or forbidden however, the transition probability of a particular spectral line can be calculated by following integrals which is known as the Fermi's golden rule which can be written as [58, 59]

$$T_{i \to f} = \frac{2\pi}{\hbar} |< f |H_{em}| i >|^2 \rho$$

Where T is the transition probability, h is the planks constant, H_{em} is hamiltonian operator for electromagnetic radiation. ψ_i and ψ_f are two atomic wave functions of hydrogen atom. ρ is the density of states.

$$H_{em} = \int \psi_f H_{em} \psi_i d\tau$$

3.1.1 Selection rules for multielectron system under various coupling scheme

The selection rules give transition probability for all the possible transitions of a system from the excited state to the lower state. Some transitions are allowed and some are forbidden according to the selection rules. Selection rules can be applied for electronic, vibrational, and rotational transitions. We basically focused on the spectra belongs to electronic transitions. In general, electric (charge) radiation or magnetic (magnetic moment) radiation can be classified into multipoles i.e ED (electric dipole), MD (magnetic dipole), electric quadrupole or electric octupole and so on. In such transitions the change in total angular momentum between the initial and final states makes several such possible multipole radiations. For example, $\Delta J = 0, \pm 1$ give rise to electric dipole transition, $\Delta J = 0, \pm 1, \pm 2$ give rise to electric quadrupole transitions etc. Usually the lowest-order multipoles dominate the transitions [60, 61, 62, 63].

In such a consideration J=L+S is considered as the total angular momentum quantum number, L is the orbital quantum number and S is the spin quantum number of the electron. In heavy atoms interaction between total angular momentum between electrons give rise to j-j coupling. According to the selection rule, during a electric dipole transition, the change in total angular momentum must be $\Delta J = 0, \pm 1$ but the transition from $J = 0 \rightarrow 0$ is not allowed. Another important quantum number is the parity (π) which needs to be inverted during any electric dipole transitions, i.e π_f and $-\pi_i$ where π_i and π_f can be denoted as the parity of initial and final state of an electron respectively. However, in light atoms

	Electric dipole transition	Magnetic dipole transition
j-j coupling	$\Delta J = 0, \pm 1$ $J = 0 \rightarrow 0$(not possible) $\pi_f = -\pi_i$	$\Delta J = 0, \pm 1$ $J = 0 \rightarrow 0$(not possible) $\pi_f = \pi_i$
LS coupling	If $\Delta S = 0$ $\Delta L = 0, \pm 1$ $L = 0 \leftrightarrow 0$(not possible)	If $\Delta S = 0$ $\Delta L = 0$

Table 3.1: selection rules for electric and magnetic dipole transition

electron spins interact to form a total spin angular momentum (S). Likewise, orbital angular momenta form a total orbital angular momentum (L). The interaction between the quantum numbers L and S is known as Russell–Saunders coupling or LS coupling. This S and L coupling gives rise to form total angular momentum J. Selection rules for a particular transition in L-S coupling impose some restrictions on the change of total orbital angular momentum and the total spin angular momentum. For the L-S coupling $\Delta S = 0$, $\Delta L = 0, \pm 1$ but $L = 0 \rightarrow 0$ is not allowed. It is shown in table 3.1 [60, 61, 62, 63].

According to the Laporte rule in a centrosymmetric environment transitions between the same atomic orbitals are forbidden. However, these transitions can be allowed if the center of inversion change by certain crystal environment [62, 63, 64, 65, 66]. In a first order approximation LS coupling model can be used for analysis of energy levels in RE ions taking in to consideration of spin orbital Hamiltonian. The eigen functions obtained are

then called intermediate-coupling wave functions [67]. An energy level scheme has been reported by Dieke *et al.*[26].

3.1.2 Term symbol for energy levels in Europium (Eu) atom and its electronic coupling scheme

The focus in this thesis is on the element Eu and the electronic states are described in the following.

The electronic configuration of Eu^{3+} is $[Xe]4f^6$. The term symbols have been used for spectroscopic notation i.e $^{2S+1}L_J$. J represented as total angular momentum, L is represented as orbital angular momentum and S is the total spin angular momentum. The lowest value of J is 0 and possible J values are from $|L+S|$ to $|L-S|$ i.e 6 to 0. Therefore L=3 and the configuration of lowest energy is $^7F_0$ with S=3, L=3, J=0. For configuration of higher J such as $^7F_1$, $^7F_2$, $^7F_3$, $^7F_4$, $^7F_5$ and $^7F_6$ the energy increases.

Using the Hund's rule, the lowest energy state can be evaluated as follows. It states [60, 61, 62, 63]

- terms with highest multiplicity (2S+1) has lowest energy
- among various multiplicity the lowest energy state has the highest L (angular momentum)
- If the sub shell is less than half filled then the lowest J value has lowest energy and if the sub shell is more than half filled then highest J has lowest energy.

  For triply ionized Eu^{3+} there are 6 electrons in the 4f shell which would be completely filled with 14 electrons. Therefore the lowest J value would be the lowest in energy. The maximum total spin will $6\times1/2$ =3, and the multiplicity is 2S+1=2*3+1=7.

3.1.3 Selection rules for RE ion in a crystal environment

RE ions doped into solid host materials give the characteristic luminescence. As previously mentioned, the rare earth ions are characterized by an incompletely filled 4f orbital which is shielded by the outer shells such as the filled $5s^2$ and $5p^6$ orbitals. As the host lattice distort the centrosymmetric environment of RE ion, these transitions named as (1) induce electric dipole transitions (ED) (2) magnetic dipole transitions (MD), and most weak (3) electric quadrupole transitions (EQ) become partially allowed [62, 63]. These electric dipole transitions are also referred as forced electric dipole transitions. Therefore to explain the europium ion spectra the crystal field must be taken into consideration. The detailed selection rules are explained elsewhere [62, 63]. Usually the emission spectra of RE ions doped in various hosts show large numbers of narrow lines. Each small group of lines corresponds to a transition between two $^{2S+1}L_J$ free ion levels, where J is considered as total angular momentum and S is considered as spin angular momentum as mentioned before. These transitions are restricted according the selection rules imposed by crystal field symmetry.

The selection rules for induced ED transitions are $\Delta L = \pm 1$, $\Delta S = 0$, Furthermore, J =0 to J= 0 is forbidden because the total orbital momentum does not change. As mentioned before according to the Laporte's parity rule ED transitions in an RE ion are strictly forbidden. The spin-orbit coupling can lift the spin selection rule. This can happen when some admixtures of different spin states occur due to crystal field [62, 63]. Therefore, the spin selection rule is relaxed and transitions are not strictly forbidden. The only allowed ED transitions are those involving a change of parity: even to odd with the spin selection rule $\Delta S = 0$ by admixing of the states. If the RE ion is located at a site that is a center of symmetry in

	S	L	J No $(0 \leftrightarrow 0)$	parity
Electric Dipole	$\Delta S = 0$	$\Delta L \leq 6$	$\Delta J \leq 6$ $\Delta J = 2, 4, 6$	opposite
Magnetic Dipole	$\Delta S = 0$	$\Delta L = 0$	$\Delta J \leq 0, \pm 1$	same

Table 3.2: Revised selection rules for electric and magnetic dipole transition

a crystal lattice, the odd crystal field terms are absent and the admixture can not lift the selection rule. When RE is located at a site where there is no inversion symmetry, the odd crystal field components will mix with opposite parity states into the $4f^n$ levels. Thus the transitions become allowed. The revised selection rules for RE ions are well described somewhere else [62, 63]. According to the revised selection rules the conditions are given in table 3.2.

In an electrostatic crystal field, the (2J+1) fold degeneracy of the free ion levels is partially lifted. The wave functions of opposite parity mixed to the crystal field levels which allow the electric dipole transitions. If the energy levels and the selection rules for a particular transitions between these levels known then the crystal field symmetry at the RE3+ site can be approximately determined [68].

3.2 Symmetry determination using europium (Eu^{3+}) spectra

The spectra of lanthanide ions in host crystals can be explained on the basis of the point group of the lanthanide site. Using the selection rules it is possible to discriminate between different point groups. The trivalent europium has an advantage of non degenerate ground state $^7F_0$. Using the selection rules all the non centro symmetric point group can be analyzed. The centro symmetric point group can not be analyzed because there is no induced electric dipole transition opposite pairity mixing. The non centrosymmetric point groups are respectively D_6h, D_3, C_{6v}, C_6, D_{3h}, C_{3h}, C_3v, C_3, D_3, D_4, C_{4v}, C_4, S_4, D_{2d}, D_2, C_{2v}, C_2, C_s and C_1. When a free ion is located in a crystalline host its spherical symmetry is broken and 2J+1 degeneracy of $^{2S+1}L_J$ multiplet is partially or completely lifted. The multiplets may be split in to number of crystal field levels.

Figure 3.1 is a site symmetry determination scheme using Eu^{3+} spectra used by several groups such as Guohua *et al.* [59], Binnemans et al[68] etc.

Among all the transitions the $^5D_0$ to $^7F_2$ and the $^5D_0$ to $^7F_1$ transitions are referred as hypersensitive electric-dipole (ED) and magnetic-dipole (MD) transitions, respectively [69, 70, 71]. When the Eu^{3+} ion is located at a certain center of symmetry, ED transitions between the 4f levels are strictly forbidden by the Laporte selection rule however, the MD transitions are allowed [70]. So, the intensity of the ED transition is strongly dependent upon the local symmetry environment around the Eu^{3+} ion, while the intensity of MD transition is comparatively unaffected by this local environment. Accordingly, the intensity ratio of ED to MD transition is known as the asymmetry ratio (R). This value would be zero when the Eu ion is at a center of an ideal symmetry, but could be quite large for distorted local environment. This ratio is a measure of the degree of distortion of the inversion sym-

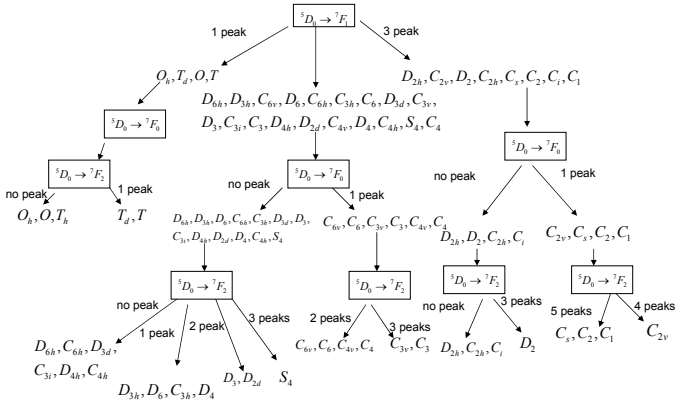

Figure 3.1: Scheme for point group determination based on Eu^{3+}transition. The weak transitions are not included here. [59]

metry of the Eu^{3+} ion site in the host lattice [69, 70, 71, 72, 13]. The asymmetry ratio of the 1.8 at percent (Eu concentration) Eu-doped GaN films is found to be 3.3 [71], Tanaka *et al.* [13] found the ratio as 12.4. For oxide material host this ratio found to be 12.8 for Y_2O_2S:Eu and 6.6 for Y_2O_3:Eu [13]. This large ratio indicates significant amount of distortion of the inversion symmetry of the Eu^{3+} lattice sites. It has been reported that the Eu^{3+} ion is incorporated into the wurtzite GaN host by substitution on the Ga sublattice, which is a C_{3v} symmetry [70].

3.3 Site multiplicity of Eu^{3+} emission

The Eu^{3+} ion is found optically active in association with neighboring intrinsic or induced defects. These complexes created a family of such optically active sites according to the crystal environment. Eu^{3+} emission involves many such centers or optical active sites in a certain hosts [73, 74, 75]. Theoretical investigation [76] found various defect complexes. Rare earth ions show a strong preference for the Ga-lattice site, either as isolated substitutional or to form complexes with intrinsic defects. The complex formed by RE_{Ga} substitutionals and vacancies or interstitials lower the symmetry and distort the local environment. For p-type GaN, the $RE_{Ga}V_N$ complex forms the most stable configuration and for n-type GaN $RE_{Ga}V_{Ga}$ complex forms a more stable pair [76]. RE_{Ga} is the substitutional rare earth ion n Gallium place, V_N is the nirogen vacancy and V_{Ga} is the Gallium vacancy. Such a family of complex sites leads to site multiplicity which is a common feature in many solid hosts. The best way to estimate the number of sites is to carefully observe the $^5D_0$ to $^7F_0$ transitions since there is no fine-structure splitting. The number of peaks in this transition range (2.10 eV) should be the number of sites in that particular host [73]. Various studies

have been performed to discriminate between the different sites. Photoluminescence excitation spectroscopy [14], combined emission and excitation spectroscopy [77] are methods for identification of different optical active sites. Another important way which we have followed to find out the different sites is to observe the temperature dependency of photoluminescence intensity of each individual peak for a particular transition. The temperature dependency of photoluminescence intensity of each individual peak of the same transitions should be the same and different for other optical active sites.

3.4 Excitation process

The excitation process of Eu^{3+} is a very complicated process. The various possible processes are described in the following sections.

3.4.1 Rare earth Impurities in Nitrides: isoelectronic trap

The isoelectronic impurities in semiconductors are termed as simple or structured impurities depending on the impurity states they introduce in the band gap [78]. The simple impurities introduce effective-mass like energy states into the crystal, in contrast to the structured impurities such as rare earth ions and transition metals introduce many-electron energy states. The structure arises due to the intra atomic transition of transition metals or rare earth metals (RE). RE ions are very chemically active so they can form more complex centers with other impurities related to implantation, *in situ* doping or with the native defects. RE impurities normally introduce localized electronic states in the semiconductor hosts, namely 4f-like states. These states are localized within the core of RE and not being involved in chemical bonding as they are shielded by outer electrons.

Rare earth doped semiconductor has been extensively investigated in recent past. Initially it was observed that small band gap semiconductors are not suitable as host at higher temperatures. For example, the quenching of erbium luminescence in silicon is quite high at room temperature [79, 80]. In contrast wide band gap semiconductor are more promising as the host material as RE luminescence do not quench significantly at room temperature. Optical properties of rare earth ions are slightly dependent on the nature of the crystal hosts as well as on temperature. Since the 4f electrons are responsible for luminescence, its properties (spectral position, energy levels etc) are similar as it were free ion [78].

Lozykowski *et al.* [78] discussed a energy transfer model and recombination process from host to RE ion. Triply charged rare-earth ions act as structured isoelectronic traps in III-V semiconductors. These rare earth ions replace the group III elements. They form trap-like states in the band gap and capture electrons or holes. It is known that the outer electron shells for rare earth ions have the form ($5s^2$ $5p^6$). The Pauli electro negativities for rare earth ions are lower than that for Ga (1.81) and is in the range from 1.1 to 1.25. Most of the rare earth ions are substitutional impurities, however they are not necessarily be pure substitutional. They can combine with native defects or located in the interstitial sites [81]. According to Thomas [82], these isoelectronic impurities in the semiconductor hosts can bound an electron or hole. The primary factors for binding potential are the electro negativities and the ionic radii between the impurity and the host ion which it replaces [81]. The formation of the bonding potential for isovalent traps may arise due to other mechanism as well [83], namely, spin orbital interaction and deformation fields in the neighborhood of the impurity. The bonding potential form by this disturbing arrangements can capture electrons or holes which subsequently form an exciton.

The energy transfer takes place from the localized state in the forbidden gap and the localized core state of rare earth impurities. There are several possible mechanism are proposed [78, 84]. First the electron/hole captured by the isoelectronic traps. Secondly, the isoelectronic trap capture another opposite charge carrier subsequently form an bound exciton. Then these excitons recombine and subsequently transfer their energy to the core electrons of the isoelectronic trap. To transfer energy the initial state and final state must be resonant otherwise excess energy distributed as phonon. As 4f core electrons are involved so the phonon coupling is very small [78].

3.4.2 Charge transfer state

It has been reported [13, 85] that the charge transfer state (CTS) of Eu^{3+} could be an important way in transferring energy from host to RE ion. The charge transfer state (CTS) of Eu^{3+} is a Eu^{2+} ion bound to a hole as following.

$$Eu^{3+} \rightarrow Eu^{2+} + h$$

The charge-transfer state of Eu^{3+} can be considered as a kind of defect related trap states as it act as as an impurity bound exciton. The electron hole pair produced after the optical excitation relaxes to the charge transfer state of Eu^{3+}, where the electron is trapped by Eu^{3+} and as the hole is bound to Eu^{2+}, the electron hole recombination energy subsequently transfer energy to excite Eu^{3+} and then it emits luminescence through the inner 4f transitions. In GaN charge-transfer state of Eu^{3+} found to be at low energy position compared to oxide hosts such as Y_2O_2S and Y_2O_3 [13, 14, 72].

3.4.3 Donor-acceptor pair related energy transfer to Eu

We propose a donor-acceptor pair related energy transfer to Eu^{3+} ion from Mg doped p-type GaN host. The detail discussion of the model is given in chapter five.

4 Experimental details:

4.1 Sample growth

Various samples (u-GaN, p-GaN, AlGaN, p-AlGaN, n-AlGaN, AlN) were grown in a low pressure metal–organic vapor phase epitaxy (LP-MOVPE) system with a horizontal reactor (Aixtron AIX 200RF). The samples having thicknesses of 1-2 μm were grown at a temperature of $\geq 1100^0$ C and a pressure of 100 mbar. We have used c-plane sapphire or c-plane 6H-SiC as substrate. Samples were grown with different doping type and concentration. In all cases magnesium was used for p-type doping and silicon for n-type doping. The precursors used were trimethylgallium (TMGa), triethylgallium (TEGa), trimethylaluminum (TMAl), trimethylindium (TMIn), ammonia (NH_3), bis(cyclopentadienyl)magnesium (Cp_2Mg) and Silane (SiH_4) for Ga, Al, In, N, Mg and Si respectively.

4.2 Ion implantation and annealing

Different kind of rare earth ions (Ce, Eu, Er) and transition metals (Cr, Ni, Co) were implanted on thin layers of u-GaN, p-GaN, AlGaN, p-AlGaN, n-AlGaN and AlN. Focussed ion beam was used for implantation. Ions were implanted with doses in the range of 10^8 cm^{-2} - 10^{14} cm^{-2} at energy 100 keV or 200 keV at room temperature. The implanatation angle was chosen to be normal to the surface of the sample. A schematics of focussed ion

beam is shown in figre 4.1. Implantation was done at Ruhr Universität, Bochum, Germany.

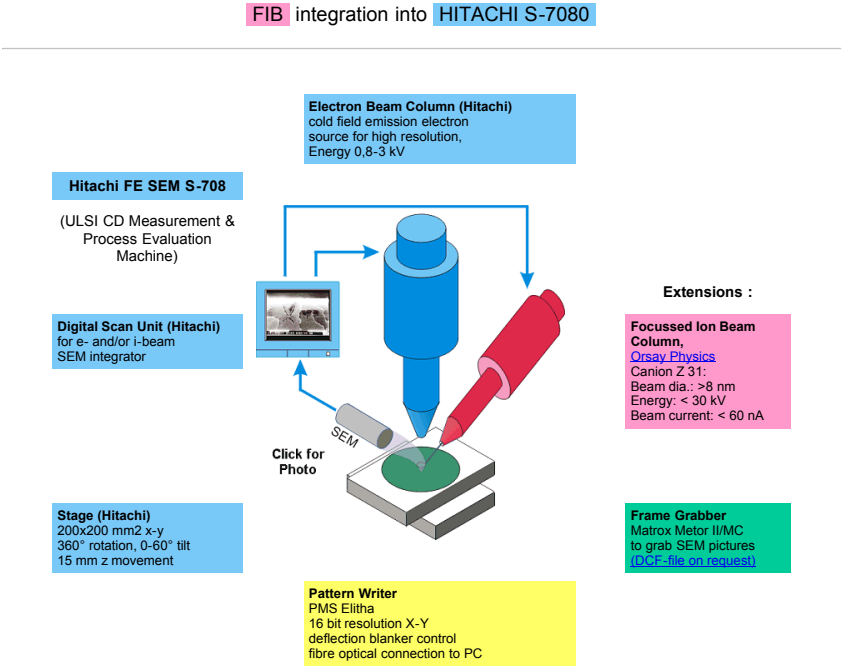

Figure 4.1: Schematics of focussed ion beam

The sources for the ions are usually liquid metal ion sources (LIMS). The liquid metal ion sources are AuEuSi, AuCeSi, AuErSi, AuBGeNi, AuCrGr and AuCoGe for Eu, Ce, Er, Ni, Cr and Co respectively. Magnetic field was applied to separate the ions and electric field was applied to accelarate the ions to higher energies. Ions are implanted within an area of

200μm x 200μm. A typical implantation plan is shown in figure 4.2.

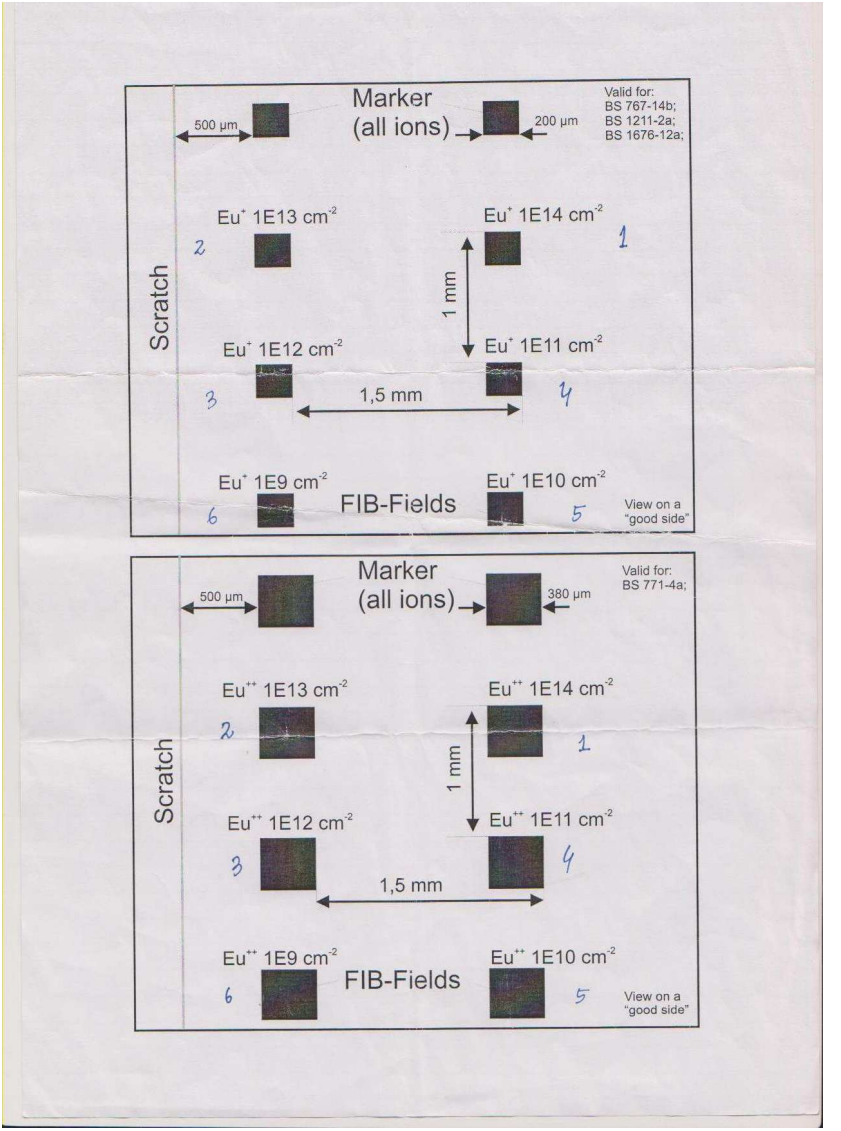

Figure 4.2: A typical image of implantation plan on GaN sample with 1 cm x 1 cm size. To find the implanted area the marker was put above the sample.

During implantation the crystal structure of the samples is damaged due to collision of energetic ions with the host atoms. To reduce the implantation damage the implanted samples were annealed at 1050^0C in nitrogen atmosphere (1 bar) for 5 minutes by rapid thermal annealing (RTA). In RTA a carbon container was used for annealing. Annealing was done by infrared lamps. Temperature in the container is controlled by a pyrometer and a thermocouple. The thermocouple is mounted on the bottom of the container close to the sample where measurement of the temperature was done by a pyrometer. Annealing was done in N_2 atmosphere (1 bar) to reduce the evaporation of nitrogen from the sample during the high temperature annealing.

4.3 Sample preparation

Samples are cleaned by some chemical reagents like aceton, methanol and deionised water. After cleaning the samples are mounted on the sample holder by a glue which can act as an adhesive even in 15 K. The sample holder along with the samples is then mounted on the cryostat.

4.3.1 Cryostat-I

The cryostat is used for cooling the sample down to 4 K using liquid helium which is composed of two co-axial cylindrical chambers. One chamber contains liquid helium on the other hand another chamber contains liquid nitrogen. The space between the two chambers remains evacuated by a turbo molecular pump for all the time down to less than 10^{-5} mbar. First liquid nitrogen is transferred into the nitrogen chamber and then liquid helium is transferred into the helium chamber by the help of a helium bridge. The helium bridge is a hollow cylindrical rod having a vacuum spacer inside it. The helium is being transfered

when there is equilibrium in pressure maintained between the helium can and the helium chamber of the cryostat. The figure 4.3 shows the schematics of the cryostat. Four windows are built in the cryostat. Through one window the laser line is incident on to the sample and through another window the emission from the sample is collected by the CCD. Using other windows, the sample can be adjusted to the right position. This type of cryostat basically associated with the He-Cd laser and Nd:VYO_4 laser system

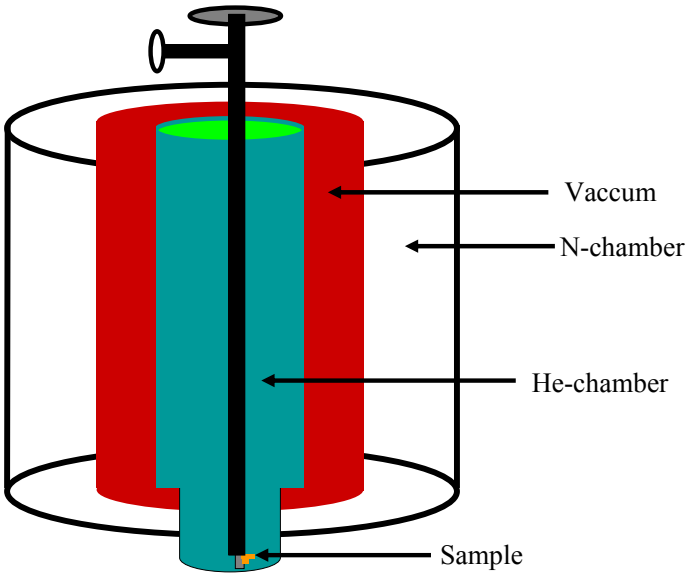

Figure 4.3: schematics of cryostat

4.3.2 Cryostat-II

The cryostat is used for cooling the sample down to 15 K using liquid helium which is composed of one cylindrical type of chamber. The chamber is made vaccum by a turbo

pump. There is a helium tube which sorrouned the sample holder. Helium is made to fill in the tube by the help of a helium bridge. The helium bridge is a hollow cylindrical rod having a vacuum spacer inside it. The helium is being transfered from the can using a He-pump. The figure 4.4 shows the schematics of the cryostat. This is associated with the Ar-ion laser system.

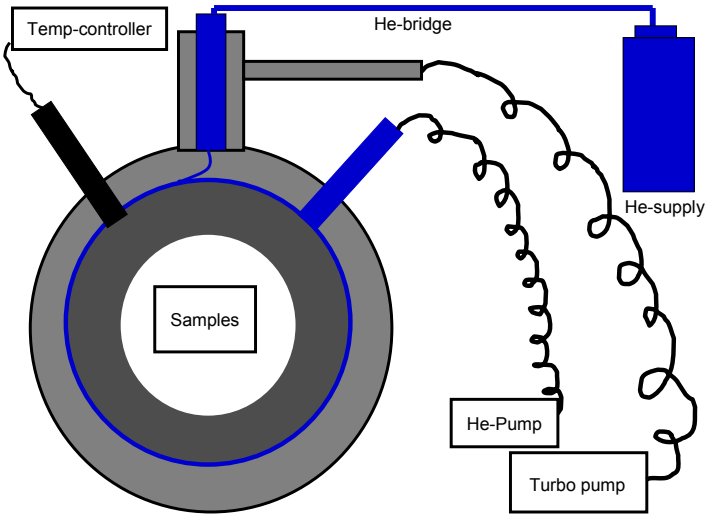

Figure 4.4: schematics of cryostat

4.3.3 Temperature controller

A thermocouple and a heater are connected to the sample holder. A temperature controller (LakeShore 330) was connected to the thermocouple and heater. Using the temperature controller one can control the temperature very near to the sample by optimizing

the P(Propotional)I(Integral)D(Derivative) parameters.

4.4 Spectroscopic technique

The photoluminescence experiments are carried out by using different kinds of laser systems. A detail sketch of the photoluminescence setup using an Ar-ion laser is shown in figure 4.5. The samples are placed in the cryostat. Mirrors, diverging lens and focussing lens are used to redirect and focus the laser light on the sample. The minimum beam diameter is approximately 50 μm. The laser light hits the sample through a cryostat window. The light emission from the sample is focused on the entrance slit of a monochromator and a Jobin-Yvon monochromator with CCD detector system (0.32 m focal length grating 600 lines/mm). The spectral resolution of the system is about 0.2 nm. A computer is connected to the CCD controller is taking the data. All the spectra were calibrated by using a Ne lamp. The figure 4.6 shows a picture of this PL setup.

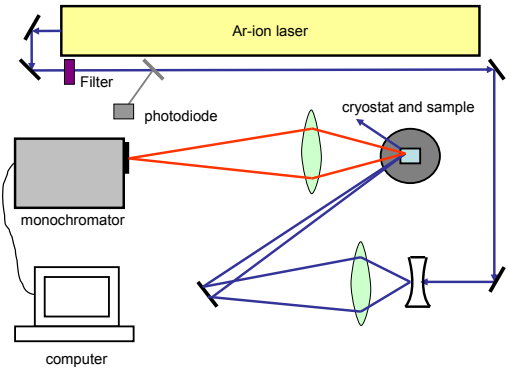

Figure 4.5: experimental setup for photoluminescence measurement

4.4.1 Ar-ion laser

The Ar-ion laser is an electrically pumped laser and it is cooled by water. The laser system operates at various laser lines for example 380 nm, 365 nm, 350 nm and 335 nm with variable excitation power density. Most experiments using the Ar-laser were done in combination with a Jobin-Yvon monochromator with CCD detector system (0.32 m focal length grating 600 lines/mm). The spectral resolution of the system is about 0.2 nm. A photodiode is installed to measure the laser power density and a filter is used in front of the laser head to block the unintentional laser emission.

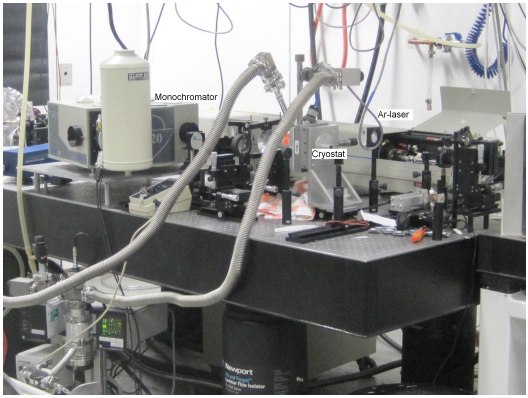

Figure 4.6: picture of Ar ion laser setup

4.4.2 He-Cd and Nd:VYO4 (vanadate) laser

He-Cd laser is a metal vapour kind of laser which is electrically pumped. The wavelength of He-Cd laser from Kimmon series is 325 nm with a power of 4 mW. Moreover another solid state laser system called Nd:VYO4 (Nd:vandate) laser from Coherent was used as well. This laser system was pumped by a diode laser. This laser emission is 1064 nm which is frequency doubled by a LBO (Lithium triborate (LiB3O5)) crystal to 532 nm. A resonant frequency doubling unit called monolithic block doubler (MBD) was installed to further doubling the frequency to 266 nm. The excitation power obtained was nearly 200 mW. The figure4.7 shows the image of Nd:vandate laser and He Cd laser.

4.4.3 Monochromator

A double monochromator spectrometer (spex 1404) was set up for detection of the emission from the samples in connection with the HeCd laser and the Nd:vanadate laser system. A nitrogen gas cooled CCD was fixed on the monochromator to detect the signal. The grating

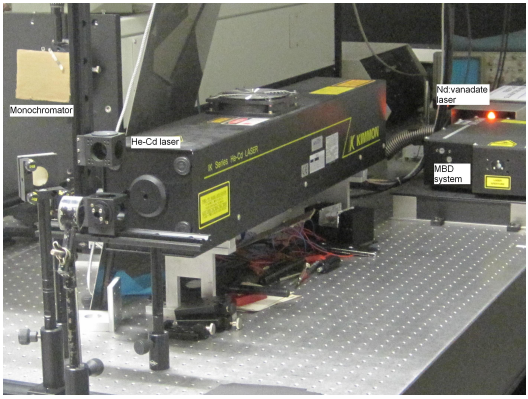

Figure 4.7: picture of He-Cd laser and Nd:vandate laser setup

used for this monochromator was 150 lines/mm. The spectral resolution of the system is about 0.8 nm.

4.5 SRIM simulation

SRIM is an abbreviation for the simulation software *The Stopping and Range of Ions in Matter* [86]. Simulation was made to determine the projection range of rare earth ions inside the nitride material after implantation by a focused ion beam. The energy of implanted ions are varying from 100 keV to 300 keV. From the simulation we found the maximum concentration of Eu ions as $10^{19}/cm^3$ with a projected range of 23 nm with a dose of $10^{14}/cm^2$. Using SRIM we determine the defect concentration due to the rare earth ion collision. In figure 4.7 and 4.8 the distribution of europium ions in GaN and AlGaN along with the vacancies created by europium ions and recoil atoms is shown respectively.

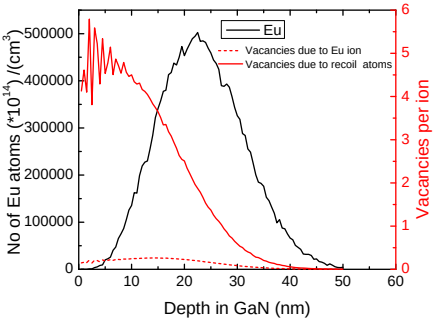

Figure 4.8: SRIM simulation of europium ion with 100 keV energy into GaN

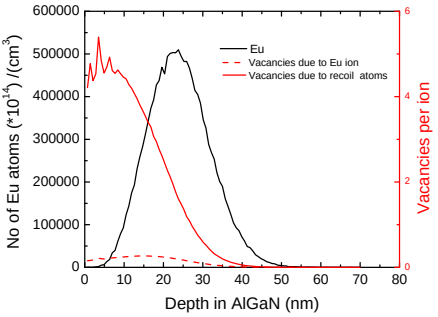

Figure 4.9: SRIM simulation of europium ion with 100 keV energy in to AlGaN

5 Results

5.1 Photoluminescence of Eu^{3+} in Mg-doped GaN:Eu

5.1.1 Identification of europium optical active centers

Figure 5.1 shows a typical Eu^{3+} photoluminescence spectrum for Mg-doped GaN:Eu in the spectral region of the peaks with highest intensity. The sample is excited by above band gap excitation of GaN at 335 nm at 15 K.

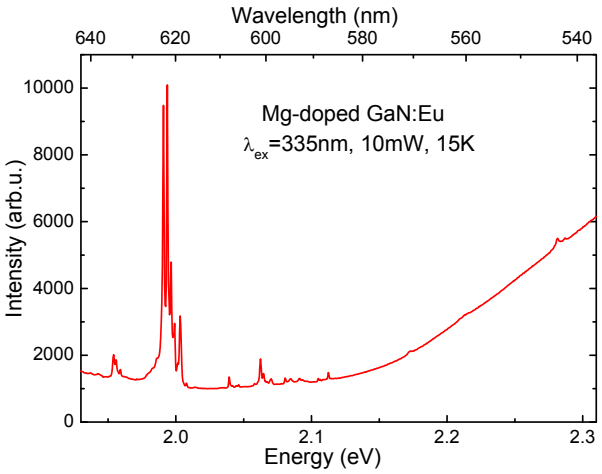

Figure 5.1: Eu^{3+} luminescence in Mg-doped GaN:Eu excited by above band gap excitation (335) nm at 15 K.

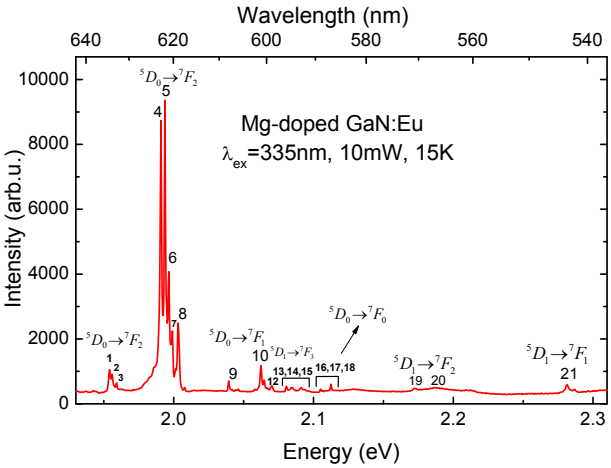

Figure 5.2: Eu^{3+} luminescence in Mg-doped GaN:Eu under above band gap excitation (335 nm) at 15 K. The spectrum is composed of about twenty peaks (numbered as 1, 2, 3 and so on) which are assigned as the transition from different excited states to different ground states. The most prominent peaks come out from the transition $^5D_0$ to $^7F_2$, which is composed of 5 lines numbered as 4, 5, 6, 7 and 8.

In figure 5.2 background luminescence which arises due to the so-called blue band in GaN [52] is subtracted. Many peaks are found in the whole spectrum. For convenience we denote them as 1, 2, 3 and so on. These peaks are very sharp having a FHWM of approximately 0.9 to 1.8 meV as shown in figure 5.3. Among all, the peaks 4, 5, 6, 7 and 8 have maximum intensity.

In figure 5.4 smaller peaks (peaks number 9 to 21) are clearly visible. All these peaks are due to electronic transitions involving the europium inner 4f orbital. These peaks are assigned according to their respective transitions comparing the spectra to earlier reports

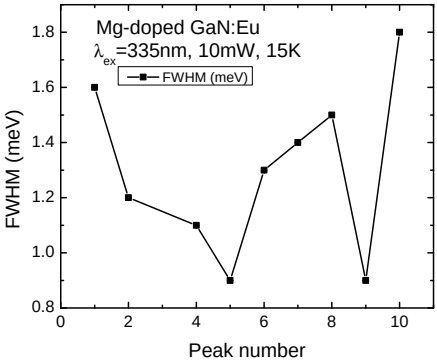

Figure 5.3: FWHM of various peaks of Eu^{3+} luminescence in Mg-doped GaN:Eu in Mg doped GaN:Eu under above band gap excitation (335 nm) at 15 K.

[68, 70, 73]. Dieke *et al.* [68] were the first to report the free Eu^{3+} ion energy level scheme. Afterwards, several authors have also investigated Eu^{3+} energy levels in different solid hosts [70, 73]. For example, Gruber *et al.* [70] have investigated Eu^{3+} luminescence in an AlN host and discussed the transitions as a consequence of split and shifted states due to the symmetry reduction by the crystal field for Eu^{3+} on an ideal Al substitutional site. Comparing their Eu^{3+} spectra in AlN to ours in Mg-doped GaN:Eu samples it is found that the spectra are very similar in shape and the peaks 4, 5 and 6 are shifted by about 7 meV towards higher energy. However, the shift is not rigid. Other peaks exhibit a smaller shift. This may be a consequence of the different lattice and the different conditions for sample preparation. Moreover, in comparison to Eu^{3+} in GaN in an another study [73], the shift of the corresponding peaks in our samples is only 0.3 meV.

Based on the assignment most peaks can be explained by transitions from the excited levels $^5D_1$, $^5D_0$ to the lower states ^7F_J (J=0, 1, 2, 3 and 4). Peaks 1, 2 and 3 are in the

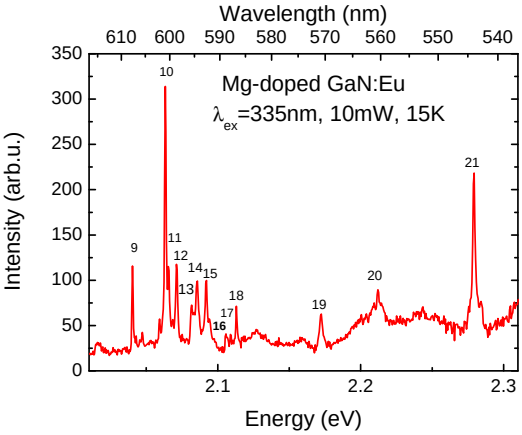

Figure 5.4: A enlarged version of photoluminescence spectrum of Mg-doped GaN:Eu in figure 5.2 for clarity of the smaller peaks numbered from 9 to 21.

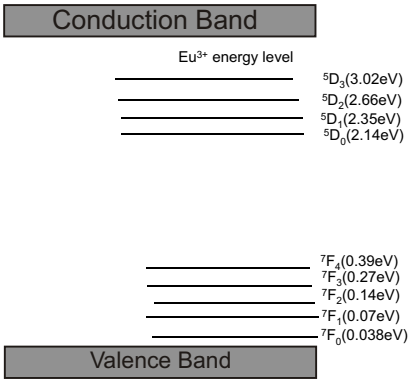

Figure 5.5: Schematic diagram of Eu^{3+} energy level scheme in GaN. The energy levels are corresponding to free ion energy levels [68, 70, 90].

range of the transition $^5D_0$ to $^7F_2$. Peaks 4, 5, 6, 7 and 8, the most intense lines, have the position found at 1.991(0) eV, 1.993(8) eV, 1.996(6) eV, 1.999(0) eV and 2.0031(4) eV respectively. These peaks are also in the range of the $^5D_0$ to $^7F_2$ transition. The degeneracy of the $^7F_2$ level of this transition is partially lifted and three lines are expected for the $^5D_0$ to $^7F_2$ transition if Eu^{3+} would be located in a C_{3v} symmetry site [87]. In case of a complete lifting of degeneracy there are five (2J+1) sub levels. But the five peaks (4, 5, 6, 7 and 8) observed in this transition range are unlikely to arise from a single optical center for reasons discussed later.

Peaks 9 and 10 are in the range of the transition $^5D_0$ to $^7F_1$. Peaks 12, 13, 14 and 15 are transitions from $^5D_1$ to $^7F_3$. Peaks 16, 17 and 18 are in the transition range of $^5D_0$ to $^7F_0$. This transition is typically forbidden for Eu^{3+} in a C_{3v} symmetry [73]. Several authors [7, 74, 88, 89, 90] have reported that multiple peaks from this transition confirm the presence of different Eu^{3+} centers. Three significant peaks are found in this transition range which indicates that three centers are responsible for emission of the whole spectrum, as described later. Peaks 19 and 20 are in the range of $^5D_1$ to $^7F_2$ transition. Peak 21 is in the range of the transition $^5D_1$ to $^7F_1$. An energy level scheme indicating all possible transitions of Eu^{3+} ion is shown in figure 5.5 [68, 70, 90].

In figures 5.6 and 5.7 the temperature dependent intensity of all the peaks originating from the excited levels ($^5D_0$, $^5D_1$) are shown. The peaks have been normalized to their maximum intensity. As shown in figure 5.6, the intensities of peaks 1, 4, 5 and 10 remain constant up to 150 K and then decreases towards room temperature. For a particular optical center, the intensity of a transition from the same excited energy level must have the same temperature dependence. So the temperature dependence of the peak intensities (1, 4 and

5), which are due to the transition from the same excited state, must be the same. Moreover, temperature dependence of the transitions belong to same optical center should also be identical if they originate from the same optical center. So peak 10 which arises due to a different excited level has a similar temperature dependency as it emerges from the same optical center. Based on these facts, it is concluded that these peaks (1, 4, 5 and 10) are likely belonging to the same optical center which is assigned as type I center.

Moreover the intensities of peak 8 remain constant with respect to temperature, shown in figure 5.7. This peak could originate from a center discussed later assigned as type III center.

In figure 5.8 the $^5D_0$ to $^7F_0$ transition for Eu^{3+} spectra in Mg-doped GaN:Eu at 15 K is shown. Three peaks (16, 17, 18) in this transition range are found. The corresponding peak positions are 2.104(9) eV (type I), 2.106(5) eV (type II) and 2.112(4) eV (type III) respectively. This transition can not be split by the crystal field due to its J=0. Therefore, the number of peaks in this transition give an indication for the same number of optically active europium centers in that particular host material [88, 89]. Observation of three peaks indicates that there are three optically active centers present in Mg-doped GaN:Eu. Along with the three significant peaks there is a shoulder (peak 17a) present in this transition range of $^5D_0$ to $^7F_0$. This could be a different optical center, however the peaks belongs to this center could not be detected.

Gruber *et al.* [70] article was taking into consideration to determine the peak position and possible optical centers. They assigned peaks as transitions from possible energy levels. Even though they have used AlN host material the comparison of difference between the peak positions in their samples and our samples should be similar. In the table 5.1 the

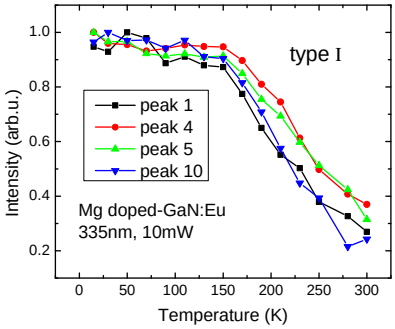

Figure 5.6: Temperature-dependent intensities for peaks 1, 4, 5 and 10 of Eu^{3+} in Mg-doped GaN:Eu by above band gap excitation. The intensities remain constant up to 150 K, then decrease toward room temperature. The peaks which have this kind of temperature dependency are belonging to one particular europium optical center, called as type I center.

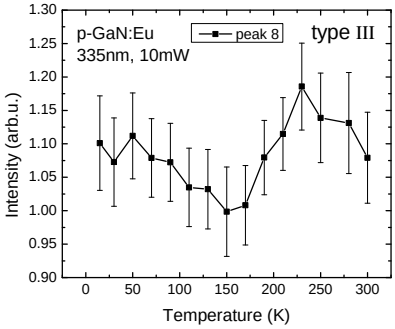

Figure 5.7: Temperature-dependent intensities for the peak 8 of Eu^{3+} in Mg-doped GaN:Eu by above band gap excitation. The intensities are constant with respect to temperature. These peaks must belong to a different center named as type III center.

difference of peak position from the corresponding peaks of their sample and in our samples was calculated. There is small differences in the values may be due to the different host material AlN which may induce a different crystal field at the europium ion site. It is clear from the these difference that peaks 1, 4, 5 and 10 belongs to one optical center named as type I center. Peaks 1, 4 and 5 are belonging to the transitions from $^5D_0$ to $^7F_2$ for this center. From the temperature dependent photo luminescence measurement it is also found that the intensity of these peaks varies in the same way. In addition, three peaks from this transition also indicate a C_{3v} symmetry site for europium ion [87]. Peak 5 and peak 6 may have contributions from other centers as reported by Woodward *et al.* [91]. So it is not possible to differentiate these peaks. Peak 7 and peak 8 do not match in to any energy levels of previous literatures [68, 70]. These peaks could be originated from different centers (type II or type III) or different transitions. However, energy difference between peak 4 and peak 16 is 114 meV, and that of peak 8 and 18 is 109 meV. For this reason peak 8 might belong to the type III center. Moreover, the peak 7 and peak 8 can not be considered as a doublet similar to peak 4 and peak 5. Because the energy difference between the peak 4 and 5 is 2.8 meV on the other hand difference between peak 7 and 8 is 4.2 meV. So peak 7 is must not belongs to type III center rather, it would be an different optical center. One peak for type III center is very unlikely for a C_{3v} symmetry site. Other peaks belong to this center peak 8 are not been observed clearly in the spectrum. They might be mix with other peaks.

Excitation power dependent photoluminescence intensities at 15 K for each peaks belong to all the above mentioned centers have been investigated and is plotted in figures 5.9 and 5.10. For the peaks of type I center the slope is found to be 0.5 as in figure 5.9, whereas for the peaks of type III center the intensities are saturating at higher excitation power as in

peak energy difference (eV)		
Difference in peak number	p-GaN:Eu (measurement)	Gruber et al.
1-4	0.03682	0.03528
4-5	0.00289	0.0017
5-10	0.068	0.070
10-16	0.0426	0.048

Table 5.1: difference in peak position with Gruber *et al.*[70] paper

figure 5.10. A possible excitation mechanism of these centers is based on a donor-acceptor pair-related resonant energy transfer which is described later in section 5.4.1.

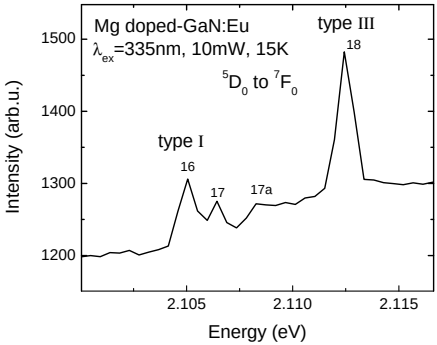

Figure 5.8: $^5D_0$ to $^7F_0$ transition spectrum of Eu^{3+} in Mg-doped GaN:Eu at 15 K by above band gap excitation. Three prominent peaks are observed along with a shoulder. Three peaks indicates the presence of three different optical centers. In addition, there is a very small shoulder like peak present near the peak corresponds to type II center. Luminescence due this center might be mixed with others and difficult to distinguish.

In figure 5.11 and figure 5.12 the temperature and excitation power dependent Eu^{3+} luminescence intensity for several peaks is shown for below band gap excitation. The intensities of all the peaks remain constant with respect to temperature and increase linearly with the excitation power. From the detailed discussion in the later part it turns out that by below-gap excitation back transfer from Eu^{3+} does not take place and the excitation process depends on the distribution of donor-acceptor pairs around the europium ion. In figure 5.12, all the peak intensities of Eu^{3+} ion are plotted against excitation power. All the peaks increase linearly with the excitation power by below-gap excitation. From the detailed discussion in the later part it turns out that by below band gap excitation the donor-acceptor pairs dominate the energy transfer process.

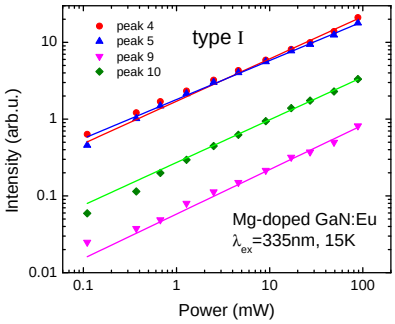

Figure 5.9: Excitation power-dependent intensities of the peaks 1, 4, 5, 9 and 10 (type I center). These peaks have square root dependence of their intensities with excitation power.

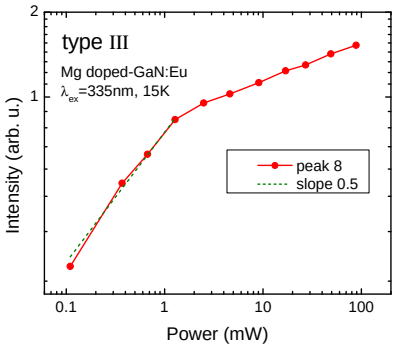

Figure 5.10: Excitation power dependent intensities of the peak 8 (type III center). The intensities are saturated at higher excitation power.

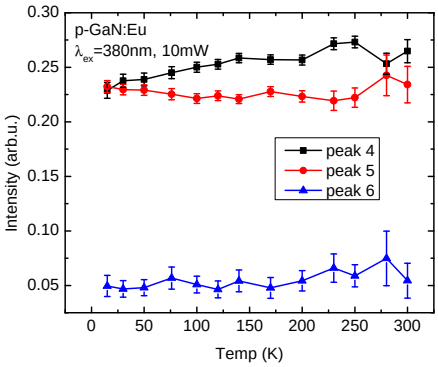

Figure 5.11: Temperature-dependent photo luminescence intensity of peaks 4, 5, 6 and 7 Eu^{3+} by below band gap excitation (380 nm). The intensities found to be constant at all temperature giving rise to a purely radiative Eu^{3+} emission.

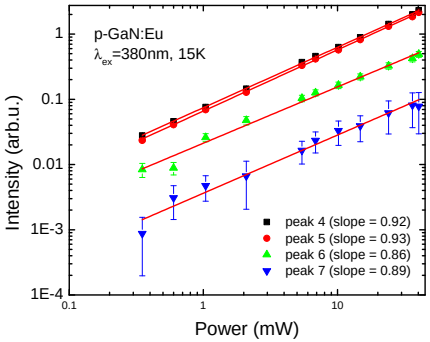

Figure 5.12: Excitation power dependent Eu^{3+} photoluminescence intensity of peaks 4, 5, 6 and 7 by below band gap excitation in Mg-doped GaN:Eu. The intensities are linearly increasing with excitation power.

5.1.2 Comparison with undoped GaN:Eu

A comparison is made for the $^5D_0$ to $^7F_2$ transition of Eu^{3+} spectra in Mg-doped GaN:Eu with that in undoped GaN:Eu in figure 5.13. The background luminescence was subtracted as before. We found the most intense luminescence peaks (4, 5, 6 and 7) in Mg-doped GaN:Eu are about three to seven times higher than in undoped GaN:Eu, depending on the Mg concentrations. In undoped GaN:Eu only three peaks (4, 5 and 6) are found in the range of the $^5D_0$ to $^7F_2$ transition.

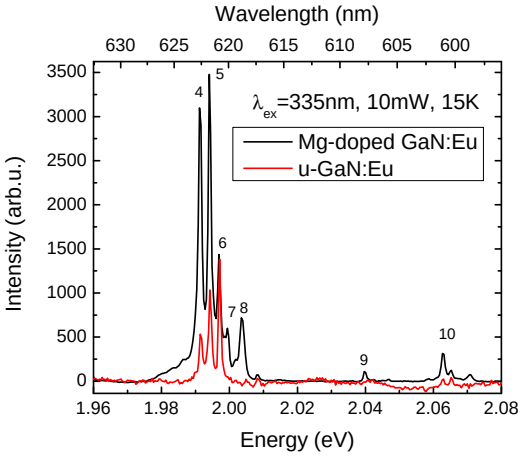

Figure 5.13: Comparison of Eu^{3+} spectra in undoped GaN:Eu and Mg doped-GaN:Eu at 15 K by above band gap excitation. More number of peaks are observed in Mg-doped GaN:Eu. Peaks 7 and 8 are not present in case of undoped GaN:Eu.

To detect which center they belong to we performed temperature dependent photoluminescence. In figure 5.14 the temperature dependent intensities of peaks 4 and 5 in undoped GaN:Eu is shown along with the same peaks of Eu^{3+} in Mg-doped GaN:Eu. The peak

intensities were normalized to their respective maximum intensities. We observed no saturation in intensities in the temperature range from 15 K to 150 K unlike in Mg-doped GaN:Eu. However, there is a similar trend in intensities found for both the peaks 4 and 5.

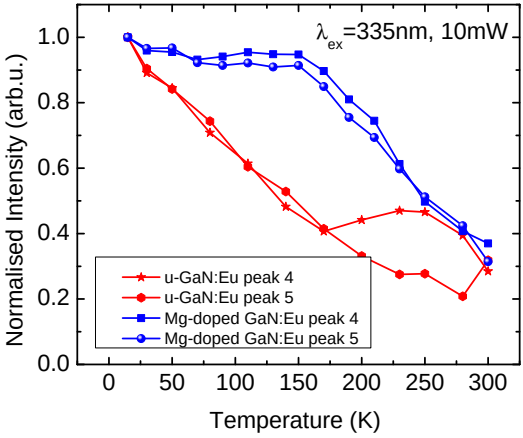

Figure 5.14: A comparison of temperature dependent normalized intensities of peaks 4 and 5 of Eu^{3+} spectra in undoped GaN:Eu and Mg doped-GaN:Eu by above-gap excitation. There is no saturation region in case of undoped GaN:Eu which indicates that Mg reduces the nonradiative centers in the temperature range 15 K to 150 K.

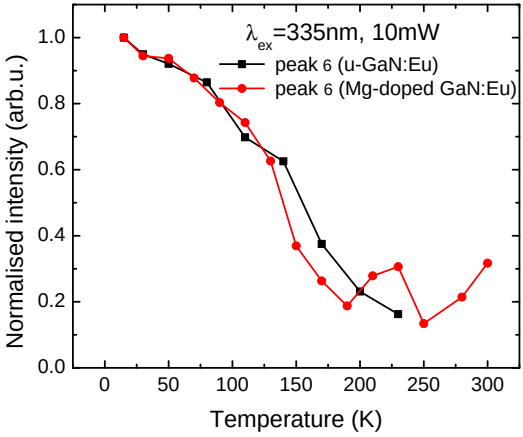

Figure 5.15: A comparison of temperature-dependent normalized photoluminescence intensity of peak 6 of Eu^{3+} spectra in u-GaN:Eu and Mg-doped GaN:Eu by above band gap excitation. The intensities are varies in a same way with respect to temperature.

This could be due to the reduction of nonradiative center on Mg doping. This confirms that peaks 4 and 5 are from the same optical center. Moreover, the intensity of peak 6 in undoped and Mg-doped GaN:Eu has a very similar trend with temperature as in figure 5.15. The origin of peak 6 is unclear as it is discussed earlier section. In undoped GaN:Eu, no such peak was found which can essentially correlate to the type III center in Mg-doped GaN:Eu. So only two types of Eu centers are present in undoped GaN:Eu, which is in agreement with the observations by O'Donnell *et al.* [74].

5.1.3 Donor-Acceptor pair (DAP) Transition in Mg-doped GaN:Eu

Donor-acceptor pairs are playing a significant role in europium excitation. Donor-acceptor pair transitions in implanted and non implanted region have been investigated. The photo-luminescence spectrum in both regions are shown in figure 5.16. The intensity of DAP transition is higher in non implanted region compared to the intensity in implanted region which could mean that the energy transfer takes place from donor-acceptor pair to europium ion.

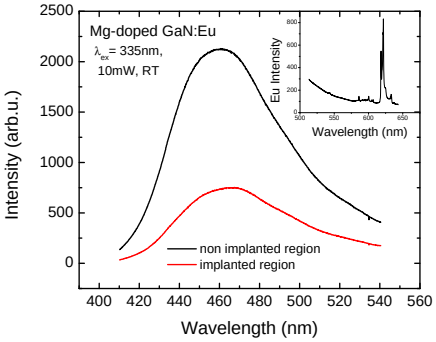

Figure 5.16: Photo-luminescence of DAP transition in Mg-doped GaN:Eu excited by 335 nm at room temperature. The spectra has taken on both implanted and non-implanted position. In the inset the Eu^{3+} luminescence in the implanted region is shown.

5.1.4 Donor-acceptor pair related energy transfer process to europium

The energy transfer from GaN to Eu^{3+} is a complex process. Several authors have tried to explain the excitation process of Eu^{3+} in different host matrices [12, 13, 14]. However, there is no complete model available in the previous literature explaining the energy transfer

mechanism from GaN to europium ions. For example, Palm *et al.* [36] reported a possible energy transfer mechanism in Er-doped Si. They assume that excitation of Er^{3+} takes place by a carrier-mediated Auger excitation process. They have observed a saturation of the Er^{3+} intensity at higher excitation power, where saturation is also observed at high excitation power but only for the peaks belong to type III center. An excitation transfer process of Eu^{3+} in Mg-doped GaN:Eu based on donor-acceptor pair (DAP) related resonant energy transfer is proposed here. The detail discussion of the model by above band gap and below band gap excitation is discussed in the subsequent sections.

5.1.4.1 Above band gap excitation

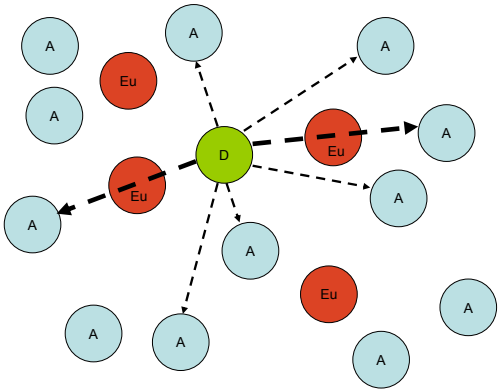

Figure 5.17: Schematics of resonant energy transfer mechanism from donor-acceptor to europium ion.

The figure 5.17 and 5.18 depicts the details of energy transfer process from GaN to Eu^{3+} ion. Here G is considered as the carrier generation rate, I_{Eu} is europium intensity (photon

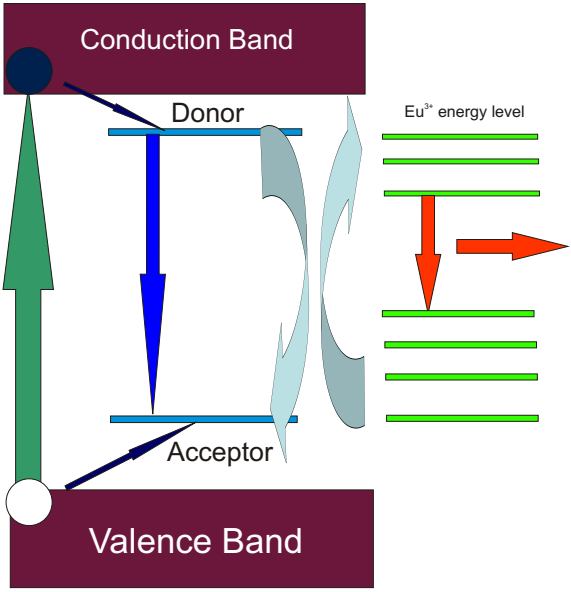

Figure 5.18: Schematic of a proposed energy transfer model by above band gap excitation. Under optical excitation neutral donor-acceptor pairs are formed. Those pairs which are at the right distance from the europium ion to transfer energy resonantly are undergoing transition. Throughout the transition they can excite the europium ions to give rise the red luminescence.

flux per second). n and p are the electron and hole densities respectively. n_0 and p_0 are density of thermally excited electrons and holes, respectively. Δn and Δp are the density of optically excited electrons and holes, respectively. N_d and N_d^0 are the concentrations of donors and neutral donors, respectively, N_{Eu} and N_{Eu}^* are the concentrations of total europium ions and excited europium ions respectively. N_a and N_a^0 are the density of acceptors and neutral acceptors which are not participating in europium excitation. N_d^{00} is the density

of thermally excited neutral donors. $N^{00}_{a,Eu}$ and $N^{00}_{a,no}$ are thermally excited europium related and non related neutral acceptors respectively. ΔN^0_d and ΔN^0_a are the optically excited donors and acceptors respectively. τ_{nr} is the lifetime of nonradiative band to band transition. τ_{rad} is the radiative life time of Eu^{3+} luminescence. N^+_d and N^-_a are the concentration of ionized donor and acceptors respectively. c_n, c_p, e_n and e_p are the capture and emission coefficients of electron and hole respectively. D and E are the transition coefficients for the transition from neutral donor to europium related and europium nonrelated acceptors respectively. Based on the proposed mechanism the rate equations has been formulated as follows

$$\frac{d\Delta n}{dt} = G - \frac{\Delta n}{\tau_{nr}} - c_n \Delta n N^+_d + e_n \Delta N^0_d \tag{5.1}$$

$$\frac{d\Delta p}{dt} = G - \frac{\Delta p}{\tau_{nr}} - c_p \Delta p N^+_a + e_p \Delta N^0_a \tag{5.2}$$

$$\frac{d\Delta N^0_d}{dt} = c_n \Delta n N^+_d - e_p \Delta N^0_a - D \Delta N^0_d N^0_a N^0_{Eu} - E \Delta N^0_d N^0_a \tag{5.3}$$

$$\frac{d\Delta N^0_a}{dt} = c_p \Delta p N^+_a - e_p \Delta N^0_a - D \Delta N^0_d N^0_a N^0_{Eu} - E \Delta N^0_d N^0_a \tag{5.4}$$

$$\frac{dN^*_{Eu,a}}{dt} = D \Delta N^0_d N^0_a (N_{Eu} - N^*_{Eu}) - \frac{N^*_{Eu,a}}{\tau_{rad}} \tag{5.5}$$

$$I_{Eu} = \frac{N^*_{Eu,a}}{\tau_{rad}} \tag{5.6}$$

$$N_d^0 = N_d^{00} + \Delta N_d^0 = \Delta N_d^0 \tag{5.7}$$

$$N_{a,Eu}^0 = N_{a,Eu}^{00} + \Delta N_{a,Eu}^0 \tag{5.8}$$

$$N_{a,no}^0 = N_{a,no}^{00} + \Delta N_{a,no}^0 \tag{5.9}$$

at steady state condition all the rates will vanish along with

$$\frac{\Delta n}{\tau_{nr}} = \frac{\Delta p}{\tau_{nr}} = 0 \tag{5.10}$$

Then from equation (5.1)

$$G = c_n \Delta n N_d^+ - e_n \Delta N_d^0 \tag{5.11}$$

Putting this value in equation 5.3 we get

$$c_n \Delta n N_d^+ - e_p \Delta N_a^0 - D \Delta N_d^0 N_a^0 N_{Eu}^0 - E \Delta N_d^0 N_a^0 = 0 \tag{5.12}$$

From equation (5.5)

$$I_{Eu} = D \Delta N_d^0 N_a^0 (N_{Eu} - N_{Eu}^*) \tag{5.13}$$

Now

$$G - I_{Eu} - E \Delta N_d^0 N_a^0 = 0 \tag{5.14}$$

$$\Rightarrow G - I_{Eu} - E \Delta N_d^0 \left(N_a^{00} + \Delta N_a^0 \right) = 0 \tag{5.15}$$

if the optically excited acceptors are very large compared to thermally excited acceptors then,

$\Delta N_a^0 >> N_a^0$ and $\Delta N_a^0 = \Delta N_d^0$ then

$$G - I_{Eu} - E\,\Delta N_d^0\,\Delta N_d^0 = 0 \tag{5.16}$$

if the europium intensity is very less in comparison to DAP transition arise due to those donor-acceptor pairs which are not exciting europium ions then, $I_{Eu} << \mathrm{E}\Delta N_d^0 \Delta N_a^0$ which leads to

$$G = E\,\Delta N_d^0\,\Delta N_d^0 \tag{5.17}$$

$$\Rightarrow \Delta N_d^0 = \sqrt{\frac{G}{E}} \tag{5.18}$$

From equation(5.13)

$$I_{Eu} = D\,\Delta N_d^0\,N_a^0\,(N_{Eu} - N_{Eu}^*) \tag{5.19}$$

$$\Rightarrow I_{Eu} = D\,\Delta N_d^0\left(N_a^{00} + \Delta N_a^0\right)(N_{Eu} - N_{Eu}^*) \tag{5.20}$$

if we assume during europium excitation the optically excited acceptors are very less compared to thermally excited acceptors,

$N_a^{00} >> \Delta N_a^0$

then putting the value of ΔN_d^0 from equation 5.18 we obtain

$$I_{Eu} = D\sqrt{\frac{G}{E}}\,N_a^{00}\,(N_{Eu} - N_{Eu}^*) \tag{5.21}$$

from equation (5.6) we get

$$I_{Eu} = \frac{N^*_{Eu}}{\tau_{rad}} \Rightarrow N^*_{Eu} = I_{Eu}\tau_{rad} \tag{5.22}$$

$$\Rightarrow I_{Eu} = D\sqrt{\frac{G}{E}}N_a^{00}N_{Eu} - D\sqrt{\frac{G}{E}}N_a^{00}I_{Eu}\tau_{rad}$$
$$\Rightarrow I_{Eu}\left(1 + DN_a^{00}\tau_{rad}\sqrt{\frac{G}{E}}\right) = D\sqrt{\frac{G}{E}}N_a^{00}N_{Eu}$$

$$I_{Eu} = \frac{D\sqrt{\frac{G}{E}}N_a^{00}N_{Eu}}{\left(1 + DN_a^{00}\tau_{rad}\sqrt{\frac{G}{E}}\right)} \tag{5.23}$$

G can be written in terms laser excitation power density as follows

$$G = CP \tag{5.24}$$

where C is a constant and P laser power, then

$$I_{Eu} = \frac{DN_a^{00}N_{Eu}\sqrt{\frac{C}{E}}\sqrt{P}}{\left(1 + DN_a^{00}\tau_{rad}\sqrt{\frac{C}{E}}\sqrt{P}\right)} \tag{5.25}$$

The excitation process can be described as follows.

1. After optical excitation, the generated carriers are captured by the donors and acceptors respectively. In a micro structural view as in figure 5.17 it is considered that a donor is surrounded by many acceptors and europium ions because acceptors and europium ions have similar concentrations which is larger than that of the donors. Donor-acceptor pair transitions takes place between neutral donor-acceptor pairs which can be considered as a dipole consisting of a positively charged donor and a negatively charged acceptors with bound electron hole pair. Among various possibility of transition of donor-acceptor pairs, only those donor-acceptor pairs can

excite europium ion which are situated at a particular distance in such a way that the excited energy levels of europium ion exactly match the donor-acceptor pair transition. This leads to a resonant energy transfer from the donor-acceptor pair to the europium ion. In addition to that there are non-radiative band-to-band transitions due to a high amount of non-radiative centers formed during implantation.

2. Europium ions are excited by resonant energy transfer from the donor-acceptor pairs. The excited europium ions can then emit red luminescence due to transitions within the 4f shell.

Equation 5.1 represents the rate of change of density of electrons generated by optical excitation which depends on band-to-band non radiative recombination, as well as capture and emission by the donors. Equation 5.2 represents the rate of the holes. Equation 5.3 denotes the rate of change of optically excited donors. This depends on electron capture and emission from donor level and the donor acceptor pairs transition (DAP) exciting europium ion and DAP transition which are not exciting europium ion. Equation 5.4 represents rate of change of acceptors. Equation 5.5 denotes the rate of excited europium ions, which depend on those donors-acceptors pairs which are resonantly transferring energy. Solving the above equations we get a square root behavior of intensity with respect to generation rate as in equation 5.25.

The fitting of this function to the experimental data for each peaks of all possible optical centers is shown in figures 5.19 and 5.20. From the equation (5.25) the denominator is

$1 + DN_a^{00}\,\tau_{rad}\sqrt{\frac{C}{E}}$

For type I center the value of $DN_a^{00}\tau_{rad}\sqrt{\frac{C}{E}}$ is 0.0038 $\frac{1}{cm^{\frac{3}{2}}\sec^2 Watt^{\frac{1}{2}}}$ which is much less compared to 1 which leads to square root dependence in intensities with excitation power.

On the other hand for type III centers this value is found to be 0.73 which lead to a saturation in intensities at higher excitation power.

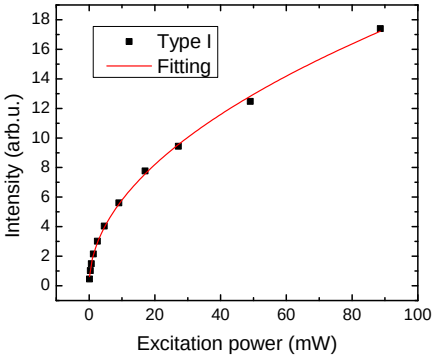

Figure 5.19: The solution of above equations is fitted to the peaks (peak 5) belong to the type I center.

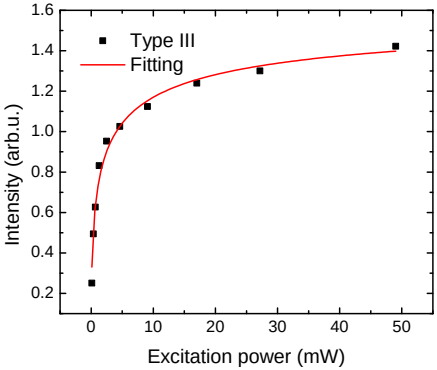

Figure 5.20: The solution of above equations is fitted to the peaks (peak 8) of the type III center.

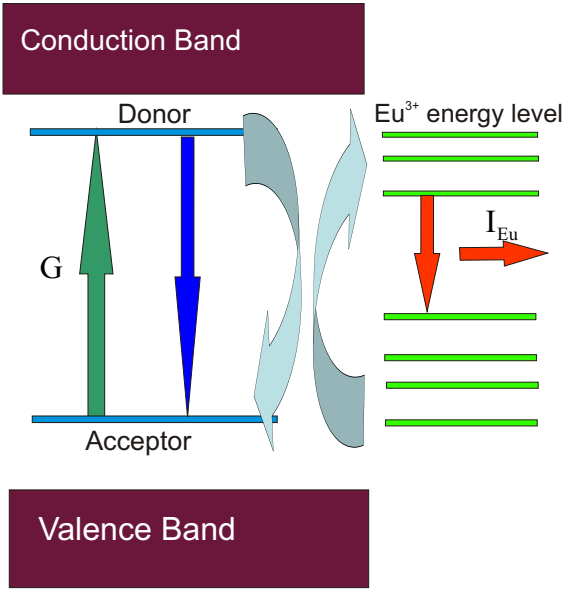

Figure 5.21: Schematic of a proposed energy transfer model under below band gap excitation. Under optical excitation neutral donor-acceptor pairs are formed. Those pairs which are at the right distance from the europium ion to transfer energy resonantly are undergoing transition. Through out the transition they can excite the europium ions to give rise the red luminescence.

5.1.4.2 Below band gap excitation

In case of below band gap excitation, donor-acceptor pairs are directly excited and subsequently transfer the energy to the europium ions as shown in the diagram 5.21.

The rate equations for below band gap excitation are the following.

$$\frac{dN_a^0}{dt} = P\left(N_a - N_a^0\right)\left(N_d - N_d^0\right) - BN_{a,no}^0 N_d^0 - CN_{a,Eu}^0 N_d^0 \tag{5.26}$$

$$\frac{dN^0_{a,no}}{dt} = P\left(N_{a,no} - N^0_{a,no}\right)\left(N_d - N^0_d\right) - BN^0_{a,no}N^0_d \tag{5.27}$$

$$\frac{dN^0_{a,Eu}}{dt} = P\left(N_{a,Eu} - N^0_{a,Eu}\right)\left(N_d - N^0_d\right) - CN^0_{a,Eu}N^0_d \tag{5.28}$$

$$I_{Eu} = CN^0_{a,Eu}N^0_d \tag{5.29}$$

$$N^0_a = N^{00}_a + \Delta N^0_a = N^{00}_a + \Delta N^0_d \tag{5.30}$$

$$\Delta N^0_a = \Delta N^0_d = \Delta N^0_{a,no} + \Delta N^0_{a,Eu}N^0_a = N^0_{a,no} + N^0_{a,Eu} \tag{5.31}$$

From the equation 5.28 and 5.29 we get

$$\begin{aligned}
&\Rightarrow N^0_{a,Eu} = \tfrac{I_{Eu}}{CN^0_d} \\
&P\left(N_{a,Eu} - \tfrac{I_{Eu}}{CN^0_d}\right)N_d = 0 \\
&\Rightarrow I_{Eu} = P\left(N_{a,Eu} - \tfrac{I_{Eu}}{C\Delta N^0_d}\right)N_d
\end{aligned}$$

for low excitation power ΔN^0_d = AP

$$\Rightarrow I_{Eu} = P\left(N_{a,Eu} - \frac{I_{Eu}}{CAP}\right)N_d \tag{5.32}$$

$$\Rightarrow I_{Eu} = \frac{PN_{a,Eu}N_d}{\left(1 + \frac{1}{CA}\right)} \tag{5.33}$$

Where P is the generation term after the optical excitation. N^0_d is the concentration of the neutral donors. N^0_a is the concentration of the neutral acceptors. N^0_a is the sum of $N^0_{a,Eu}$ and $N^0_{a,no}$. $N^0_{a,Eu}$ is the concentration of those neutral acceptors which are at the right distance from the europium ions to excite them. $N^0_{a,no}$ are the concentration of those

neutral acceptors which are not exciting europium ions, but they can participate in donor-acceptor pair recombination. $N^0_{d,Eu}$ is the concentration of the neutral donors which are participating in exciting the europium ions. B is the coefficient of transition between N^0_d and $N^0_{a,no}$. C is the coefficient of transition between N^0_d and $N^0_{a,Eu}$. P is the laser power. N^*_{Eu} is the concentration of the excited europium ions, τ_{rad} is the europium radiative life time. Excitation of the europium ions depend on those donor-acceptor pair transition which are located at a right distance to match one of the excited energy levels of the europium ion. Solution of the above equations is a linear function as in the equation (5.33) .

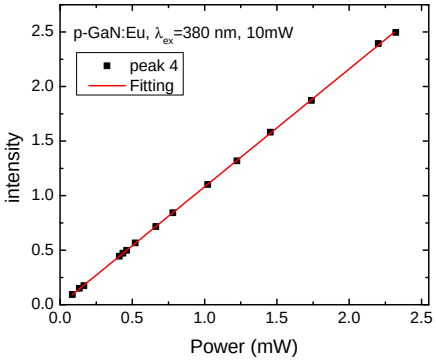

Figure 5.22: Excitation power dependent photoluminescence intensity of Eu^{3+} spectra (peak 4) in Mg-doped GaN:Eu. Other peaks (5, 6 and 7) have similar behavior. Solid line is the fitting of the data with the proposed donor-acceptor pair-related energy transfer model. The dependence in Eu^{3+} intensity is linear with increasing excitation power.

In figure 5.22 the experimental data have been fitted.

5.1.5 Temperature dependent photoluminescence of type I center

5.1.6 Luminescence quenching and non radiative process of Eu^{3+} ion

5.1.6.1 Above band gap excitation

For type I center the quenching mechanism is fitted with following Arrhenius equation (5.34) [92] shown in following figures.

$$I_{Eu}(T) = \frac{I_{Eu}(0)}{1 + A\exp\left(\frac{-E_A}{k_B T}\right) + B\exp\left(\frac{-E_B}{k_B T}\right)} \tag{5.34}$$

Here $I_{Eu}(0)$ is the intensity at low temperature, and I_{Eu}(T) is the intensity of the respective peaks at higher temperatures. k is the Boltzmann constant and T is the temperature. Two activation energies 106 meV and 0.6 meV are found which are very close to acceptor activation energy. This is a further confirmation that the excitation and de-excitation process of europium ions are due to DAPs.

Intensities of peak 8 belongs to type III center is found to be constant from 15 K to 300 K. In addition for the peaks of type I site there is a strong temperature dependence in the intensity. Similar activation energies for the peaks (peak 4 and peak 5) of type I site are found. For peak 4 the activation energies are 106 meV and 1 meV respectively and for peak 5 the activation energies are 108 meV and 2 meV respectively. The fitting is shown in figure 5.23 and 5.24.

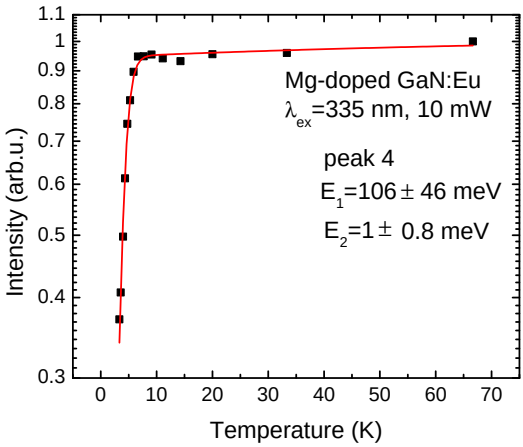

Figure 5.23: Normalized temperature dependent Eu^3+ intensity of peak 4 fitted by Arrhenius equation(5.34). The activation energies are 106 meV and 1 meV respectively

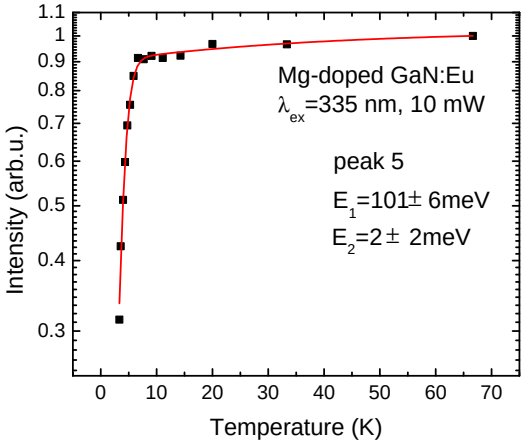

Figure 5.24: Normalized temperature dependent Eu^3+ intensity of peak 5 fitted by Arrhenius equation(5.34). The activation energies are 108 meV and 2 meV respectively

5.1.7 Below band gap excitation

For below band gap excitation the the donor-acceptor pairs are excited directly by optical excitation. Interestingly any thermal quenching of the Eu^{3+} luminescence peak intensities is not observed up to room-temperature as shown in figure 5.11, which means that there is no nonradiative process associated with temperature. This purely radiative emission from Eu^{3+} ion can be a consequence of the excitation and de-excitation process. As the donor-acceptor pairs are directly excited by below band gap excitation, a linearly increase in Eu^{3+} intensity is expectedly observed. From the emission spectra of DAP transition and Eu^{3+}, it is apparent that the difference between the DAP and Eu^{3+} energy levels is sufficiently large (approximately 800 meV) which could lead to high activation energy to observe in Eu^{3+} luminescence and that is why the back transfer energy from Eu^{3+} ion to the donor-acceptor pair is negligible giving rise to a constant Eu^{3+} emission intensity at all temperatures.

5.1.8 Constant photoluminescence lifetime of Eu^{3+} luminescence in Mg-doped GaN:Eu by below band gap excitation

In figure 5.25 the lifetimes have been determined by time resolved photo-luminescence spectroscopy at different temperatures in the spectral range of 620 nm to 624 nm. First the signal was measured at implanted spot and then at off implanted spot. To get the real contribution from europium emission I subtracted the signal from the implanted spot to off implanted spot. Lifetimes have been determined by fitting the complete transients to a mono exponential increase and decay with similar time constants by following equation

$$I(t) = I_0 + I_{steadystate} \left[\begin{array}{l} \Theta(t-t_0)\,\Theta\left(t_0+t_{pulse}-t\right)\left(1-e^{\left(\frac{-t-t_0}{\tau}\right)}\right) \\ +\Theta\left(t-t_0-t_{pulse}\right)\left(1-e^{\left(\frac{-t_{pulse}}{\tau}\right)}\right)\left(e^{\frac{-t-t_0-t_{pulse}}{\tau}}\right) \end{array} \right] \tag{5.35}$$

Where I_0 is the back ground intensity, $I_{steadystate}$ is the intensity at steady state, Θ is the heavyside function. t_0 is the time when laser turn on, t_{pulse} is the pulse width of laser. First term in side the bracket represents intensity in the rise and second term represents the intensity decay regime. The lifetime is found to have a small temperature dependence, i.e

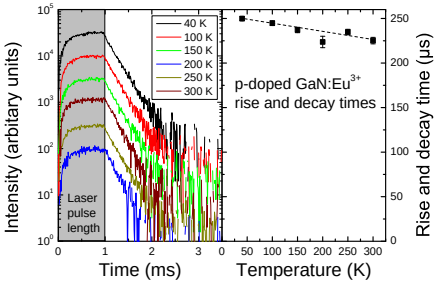

Figure 5.25: Photoluminescence lifetime of Eu^{3+} spectra in Mg-doped GaN:Eu from 40 K to 300 K. The excitation source is a 378 nm diode laser with a repetition rate of 250 s^{-1}. Left side of the figure showing the transients on the other hand right side is showing the lifetime at various temperatures. The dotted line is a guide to the eye.

250 μs to 225 μs, from low temperature to room-temperature which is shown in figure 5.25 but no sharply decrease as previously has observed [7]. However the intensity remains constant with increasing temperature. This means there is no back energy transfer taking place from excited Eu^{3+} ion to the host. Lee *et al.* [7] observed a sharp decreasing trend of life time with increasing temperature under above the band gap excitation. They explained there might be an energy back transfer with higher temperature. In our case any back energy transfer at higher temperature is not observed as intensity remains constant as in figure 5.11 which means a purely radiative emission from Eu^{3+}.

5.1.9 Effect of Mg concentration on Eu^{3+} luminescence

Eu^{3+} luminescence in GaN:Eu with Mg doping with different concentrations was investigated. The intensities of all the peaks are increasing first, then decreasing and then again increasing for increasing in Mg concentrations. The variation of Eu^{3+} intensity with Mg flux is shown in figure 5.26. This random variation of Eu^{3+} luminescence intensity may be due to the inhomogeneous distribution of Mg in GaN.

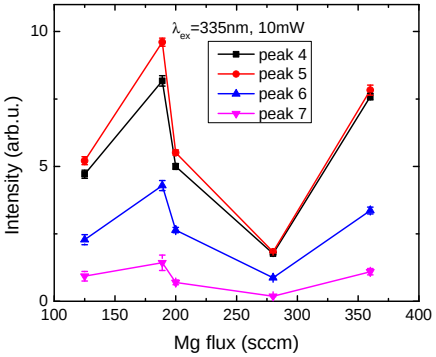

Figure 5.26: Peak intensities of Eu^{3+} luminescence in GaN with various Mg concentration. The excitation source is above band gap excitation (335 nm) at 15 K

5.1.10 Eu^{3+} luminescence for different Eu doses in Mg-doped GaN:Eu

Europium luminescence at different implanted doses from 10^{10}cm^{-2} to 10^{14} cm^{-2} was studied. Similar spectra for all doses is observed as shown in figure 5.27. However, peak 8 disappear in lower doses. The intensities of the peaks slowly increase up to the dose 10^{13}

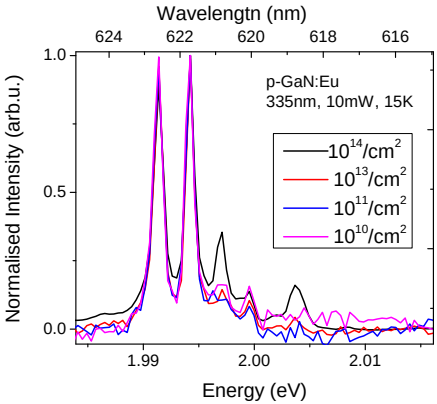

Figure 5.27: Dose dependent Eu^{3+} luminescence spectra at 15 K under λ_{ex}=335 nm excitation. The spectra are normalised to their maximum intensity.

cm^{-2} however, intensities rapidly increase for the dose 10^{14} cm^{-2} as shown in figure 5.28. This can be explained by activation of a new optical center at higher doses.

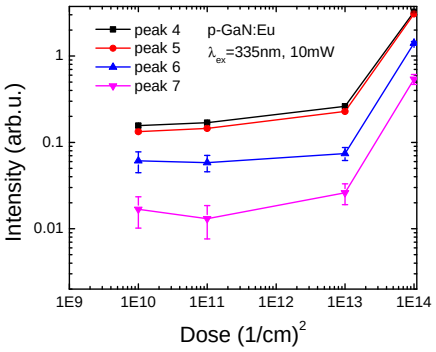

Figure 5.28: Intensities of the individual peak of Eu^{3+} in various doses at 15K for λ_{exc} = 335 nm.

5.2 Enhanced Eu^{3+} luminescence in GaN:Eu by Mg and Si codoping

As donor-acceptor pairs involved in the energy transfer to europium ion, the donor concentration was increased by Si doping in GaN. The Eu^{3+} luminescence in europium implanted GaN codoped with both Mg and Si (Mg and Si doped GaN:Eu) is investigated. Strong enhancement of Eu^{3+} luminescence was observed in these sample (Mg, Si doped GaN:Eu). The Eu^{3+} intensity in the $^5D_0$ to $^7F_2$ transition region is found to be thirty times higher compared to europium-implanted undoped GaN (GaN:Eu). The major contribution to this overall enhancement is due a weak peak (peak 8) present only in europium-implanted Mg-doped GaN at 2.0031 eV (618.9 nm) which is strongly enhanced by codoping both Mg and Si.

In figure 5.29 photoluminescence spectra for europium-implanted GaN (GaN:Eu) undoped and co-doped with Si, Mg, and both Si and Mg are shown in the spectral range of the $^5D_0$ to $^7F_2$ transition. From all spectra, the background has been subtracted. The sam-

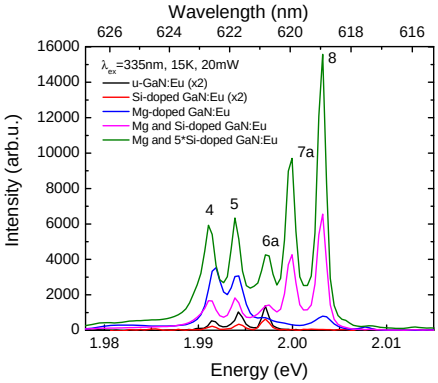

Figure 5.29: Photoluminescence spectra of Eu^{3+} in Si-doped, Mg-doped, and (Mg and Si)-doped GaN:Eu at 15 K excited by the 335 nm line. The spectra were measured under the same conditions and thus the intensities are comparable. The donors play a significant role in Eu^{3+} luminescence and as the introduction of Si (donor) is enhanced the luminescence so its concentration has been increased to five times.

ples have been excited by the 335 nm line (3.70 eV), which is well above the band gap of GaN (E_g= 3.5 eV) at 15 K. The three peaks 4, 5 and 6 are typical peaks of Eu^{3+} ions in europium-doped GaN. For undoped or Si-doped GaN:Eu the Eu^{3+} luminescence is found to be less efficient compared to Mg-doped GaN:Eu. Peak 6 has the highest intensity in Si-doped GaN:Eu, on the other hand it is found to be the least intense peak in other samples. The Eu^{3+} luminescence in Mg-doped GaN:Eu is approximately four times more intense than in undoped GaN:Eu or Si-doped GaN. Two new weak peaks 7 and 8 are emerging by Mg codoping. However, for samples doped with both Mg and Si these new peaks are enhanced more than ten times compared to the corresponding peaks in Mg-doped GaN:Eu. This could be due to a particular center being active when both Mg and Si are codoped to

GaN. The overall intensity in the range of the $^5D_0$ to $^7F_2$ transition is three times higher than in Mg-doped GaN:Eu. In case of Mg-doped and Mg and Si-doped samples the spectra are fitted by five Lorentzians and for the broad shoulder we have used a Gaussian function. From the fitting the peak positions of 4, 5, 6, 7 and 8 peaks are found to be 1.991 eV, 1.993 eV, 1.9973 eV, 1.9997 eV and 2.0031 eV respectively. However, peak 6 and peak 7 are shifted about 1 meV from that of Mg-doped GaN:Eu. So they are represented as 6a and 7a. The peaks 7a and 8 are the most intense peaks in Mg-doped and in Si-doped GaN:Eu. In addition to that, the intensity ratios of different peaks are not same for all samples, which means that these peaks are likely have contributions from different optical centers.

In figure 5.30 the $^5D_0$ to $^7F_0$ transition is shown. As discussed before this transition can not be split by symmetry, so the number of peaks represents the number of optical centers in the host. We have seen that one of the peak corresponds to the peak 18 of Mg doped GaN:Eu is significantly enhanced in the Si and Mg codoped GaN:Eu, which means that a particular Eu center is activated by Si and Mg codoping. As discussed before the peak 4 and peak 5 are belonging to a same optical center however, origin of peak 6 is unclear. In contrast to Mg-doped GaN:Eu, peak 7a and peak 8 seem to originate from same optical center and belongs to a center which correspond to peak 18.

This is confirmed by observing similar temperature dependent photoluminescence intensity of these three peaks as shown in figure 5.31

5.2.1 Below band gap absorption

In figure 5.32 the excitation wavelength dependent Eu^{3+} luminescence in Mg and Si-doped GaN:Eu both at 15 K and RT is shown. The excitation sources were chosen such that it can vary from below band gap to above band gap of the GaN host. For all excitation wavelength

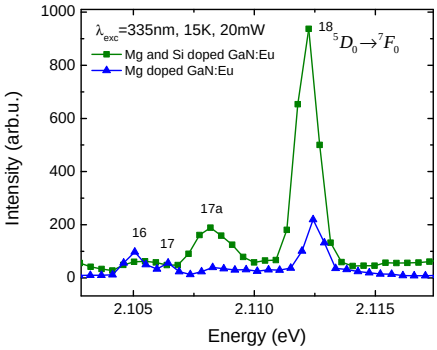

Figure 5.30: $^5D_0$ to $^7F_0$ transition of Eu^{3+} luminescence in (Mg and Si)-codoped GaN:Eu and in Mg-doped GaN:Eu at 15 K.

except 405 nm peak 4 and peak 5 have been found to have maximum intensity. The overall Eu^{3+} luminescence intensity is found to be maximum at 365 nm (3.39 eV) excitation wavelength, which is below the band gap for GaN (3.5 eV) at 15 K. In figure 5.33 the intensity ratio of peak 8 and peak 4 is plotted against excitation wavelength. The intensity of peak 4 is found to be essentially constant irrespective of excitation wavelength so it is assumed that this intensity ratio of peak 8 and peak 4 could relate to the excitation process. This ratio is increasing with increasing excitation energy towards the band edge i.e up to 3.39 eV then it is decreasing for higher excitation energy. This means that europium ions are excited by some shallow defects which are close to the band edge. These defects are excited, directly by the laser excitation or through the bandedge and transfer energy to the europium ions. As the Eu^{3+} intensity is highest if both donors and acceptors are present with large concentrations, it appears likely that this energy transfer proceeds via donor-acceptor pairs. It is envisioned that direct resonant dipole-dipole interaction between donor-acceptor pairs and excited states of Eu ions is responsible for energy transfer.

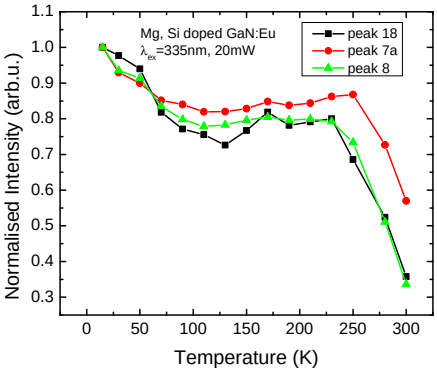

Figure 5.31: Temperature dependent photoluminescence intensity of peaks 7a, 8 and 18 of Eu^{3+} luminescence in (Mg and Si)-codoped GaN:Eu and in Mg-doped GaN:Eu.

At 405 nm excitation the intensity ratio of peaks 7a, 8 and peaks 4, 5 is smaller than unity which indicates that the optically active centers associated with peaks 4 and 5 are excited by a different pathway, possibly via deep donor-acceptor pairs present in Mg-doped GaN giving rise to the well known blue luminescence [49].

5.2.1.1 Further confirmation of Mg and Si role in energy transfer by temperature dependent below band gap excitation

In figure 5.34 the temperature dependent intensities of individual peaks of Mg and Si doped GaN:Eu are shown. The samples are excited by 380 nm laser line which is below band gap for GaN. The intensity of most intense peaks 7a and 8 increase up to 180 K then decreases towards 300 K.

As the most intense peak is a concern so the intensities of peak 8 as a function of tem-

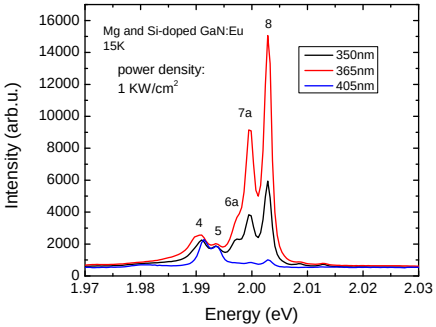

Figure 5.32: Excitation wavelength dependent photoluminescence intensity of Eu^{3+} in (Mg and Si)-codoped GaN:Eu. For all cases the power density is about 1 KW/cm^2.

perature is shown in figure 5.35. It is fitted by the analytical equation 5.36.

$$I_{pl} = \frac{I_0 + Be^{\frac{-E_1}{KT}}}{1 + Ce^{\frac{E_2}{KT}}} \tag{5.36}$$

Where, I_0 is the Eu^{3+} photoluminescence intensity at 15 K, I_{pl} is the intensity at subsequent temperatures; E_1 and E_2 are the two activation energies, B and C are the prefactors, k is the Boltzmann constant and T is the temperature. The activation energies are found to be 14$\pm$1 meV and 174$\pm$7 meV respectively.

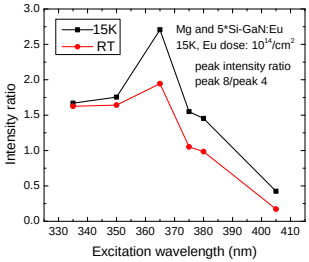

Figure 5.33: Intensity ratio of peak 8 and peak 4 of Eu^{3+} versus excitation wavelength in (Mg and Si)-codoped GaN:Eu at 15 K and RT.

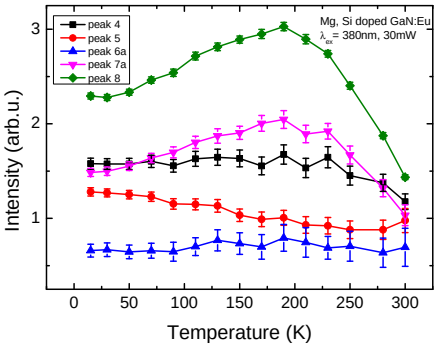

Figure 5.34: Eu peak intensities with temperature excited by 380 nm.

In figure 5.36 spectra of DAP luminescence of Mg and Si doped GaN:Eu at 2.8 eV is shown at 15 K. The intensities with respect to temperature has been fitted with equation 5.32 shown in figure 5.37. We have determined two activation energies for the DAP transition. One is 17±13 meV for the low temperature range another is 239±40 meV for high temperature range. The thermal activation energy at high temperature range usually assigned as the activation of Mg acceptor. Similar activation energies have been found for Eu^{3+} luminescence as well. This indicates that donor-acceptor pairs involves in energy transfer to the

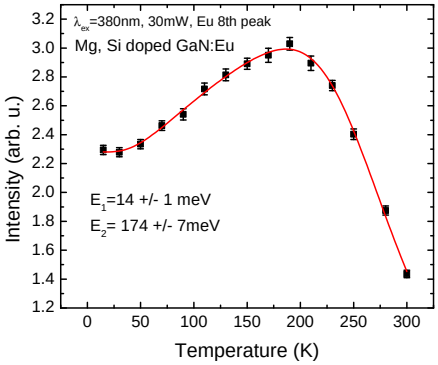

Figure 5.35: Fitting of temperature dependent intensity under below band gap excitation europium ion.

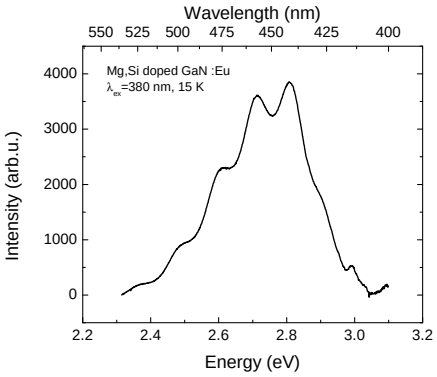

Figure 5.36: DAP luminescence in Mg,Si doped GaN:Eu at 15 K under above band gap excitation

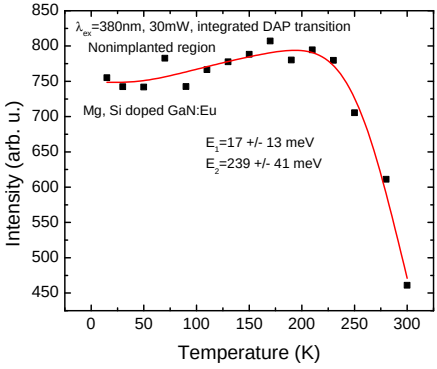

Figure 5.37: Fitting of DAP luminescence intensity with temperature

5.2.2 Temperature dependent Eu^{3+} luminescence in Mg and Si doped GaN:Eu

5.2.2.1 One nonradiative channel under above band gap excitation

In figure 5.38 the Eu^{3+} luminescence spectra is shown in different temperatures (15 K to 300 K). For all the temperatures the intensities of peak 7 and peak 8 remain highest which is reason for concerning these peaks. In figure 5.39 I fit the data with Arrhenius equation (5.34) to determine the activation energies and found that only one dominant non-radiative channel associated with Eu^{3+} luminescence in Mg, Si doped GaN:Eu having activation energy of 364 meV.

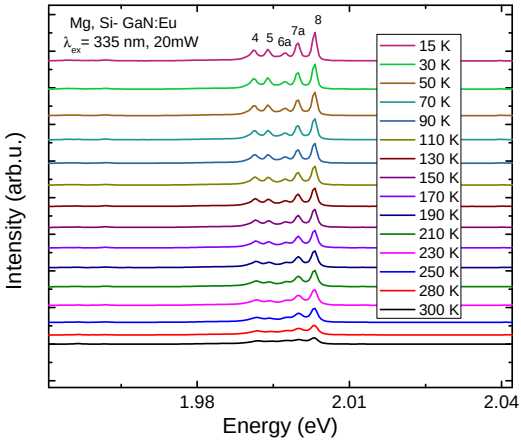

Figure 5.38: Photoluminescence of Eu^{3+} in Mg and Si co-doping in GaN under 335 nm excitation at 15 K.

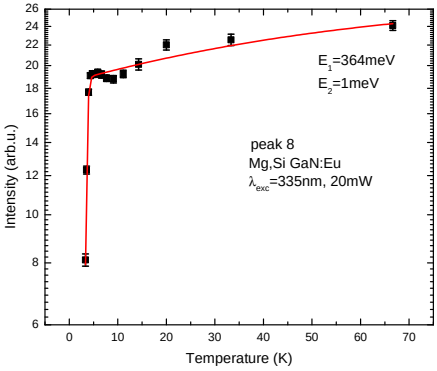

Figure 5.39: Temperature dependent intensities of peak 8 of Eu^{3+} luminescence in Mg and Si doped GaN:Eu excited by 335 nm laser

5.2.3 Excitation mechanism of Eu^{3+} ion under above band gap excitation

The peaks 7a and 8 which are emerging in consequence of Mg and Si codoping in GaN:Eu was investigated by excitation power dependent photo-luminescence at different temperature range. The intensities of peak 8 against excitation power from low to high temperature shown in figure 5.40. Similar slope (0.6) of intensities with respect to excitation power have been found for all the temperatures which is well agreement to our previous discussion of donor-acceptor pair related energy transfer model as in equation (5.25).

The fitting is shown in in figure5.41. From the fitting parameter $DN_a^{00}\tau_{rad}\sqrt{\frac{C}{E}}$ is found to be 0.05 $\frac{1}{cm^{\frac{3}{2}}\sec^2 Watt^{\frac{1}{2}}}$ which is smaller than that of the corresponding peak in Mg doped-GaN:Eu. This could be due to the involvement of different kind of donors in europium excitation.

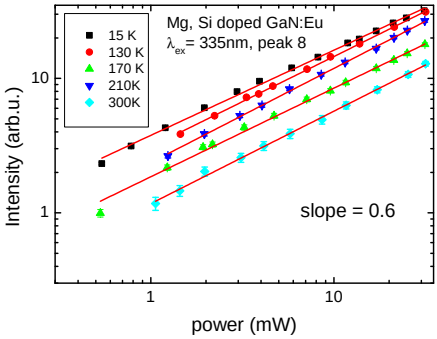

Figure 5.40: excitation power dependent of Eu^{3+} peak 8 in Mg, Si doped GaN:Eu excited by 335 nm with different temperature. The slope is found to be 0.6

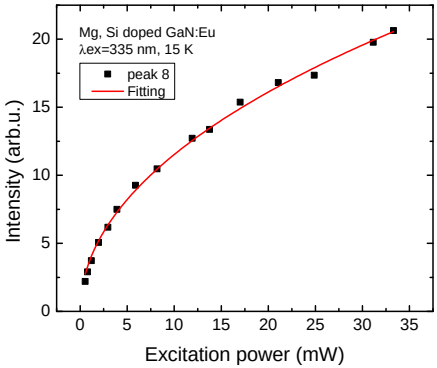

Figure 5.41: Fitting of the power dependent photoluminescence with the proposed model as in equation (5.25)

5.3 Eu^{3+} luminescence in europium-implanted AlGaN alloy

We have investigated Eu^{3+} luminescence in AlGaN:Eu with various Al composition ($Al_{0.07}$GaN:Eu, $Al_{0.20}$GaN:Eu, AlN) at 15 K which is shown in figure 5.42. The excitation source is 335 nm laser line, which is very close to the band edge in case of 7 percent of aluminium composition at 15 K. The Eu^{3+} luminescence spectra in AlGaN differ from Mg doped-

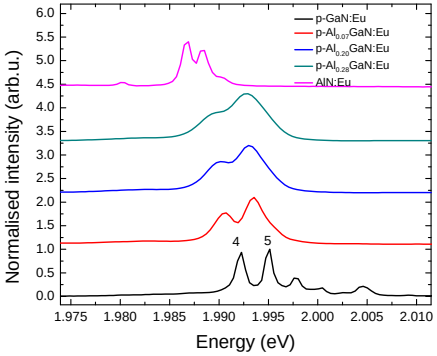

Figure 5.42: Eu^{3+} luminescence spectra in AlGaN:Eu with different Al composition along with in Mg doped GaN:Eu at 15 K. The samples were excited by 335 nm laser line.

GaN:Eu. Only the corresponding peaks 4 and 5 of Mg doped-GaN:Eu are cleary seen in AlGaN:Eu. The ratio of intensities between these peaks in Mg doped-GaN:Eu are changed in AlGaN:Eu. The number of peaks for $^5D_0$ to $^7F_2$ transition are reduced to two in case of AlGaN host. Spectra of Eu^{3+} in all investigated materials is shown in figure 5.42. The peak positions are shifted towards red with increasing Al composition as shown in figure 5.43.

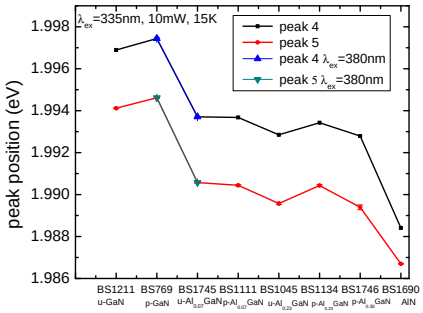

Figure 5.43: Variation of Eu^{3+} luminescence peak position (corresponding peaks 4 and 5 of Mg doped-GaN:Eu) in different Al composition.

By changing the alloy composition the crystal field of Eu^{3+} is changed and consequently the peak positions and spectral shape. The full width at half maximum (FWHM) of Eu^{3+} luminescence peaks in whole Al composition range is shown in figure 5.44. The highest FWHM was found at 30 percent of aluminium. The asymmetrical variation in FWHM as a function of composition also observed by Wang *et al.* [93]. They reported that this behavior is similar to the bound exciton luminescence in semiconductor alloys.

5.3.1 Temperature dependence of Eu^{3+} luminescence in AlGaN:Eu

5.3.1.1 one non-radiative channel under above band gap excitation

Temperature dependence of Eu^{3+} luminescence has been studied under above and below band gap excitation sources and is shown in figure 5.45. The data is fitted with Arrhenius equation (5.34). One dominant activation energy of 142 meV is found which is responsible for intensity quenching. The fitting is shown in figure 5.46.

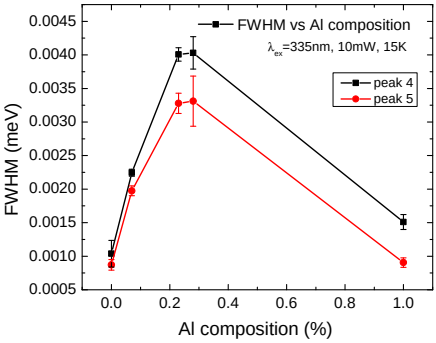

Figure 5.44: FWHM of Eu^{3+} luminescence peak in whole Al composition range.

5.3.1.2 Temperature dependence Eu^{3+} luminescence in AlGaN:Eu under below band gap excitation

In case of below band gap excitation the Eu^{3+} luminescence remains constant similarly as in Mg doped GaN:Eu. The intensity as a function of temperature is shown in figure 5.47.

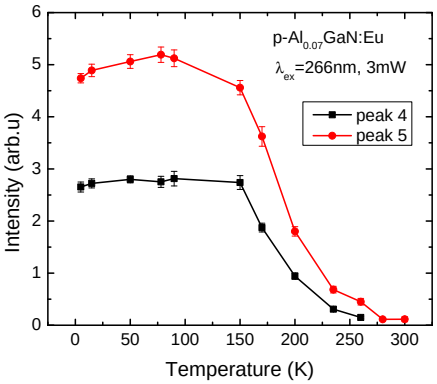

Figure 5.45: Temperature dependent peak intensities of Eu^{3+} luminescence in AlGaN:Eu

5.3.1.3 Photoluminescence lifetime of Eu^{3+} luminescence in AlGaN:Eu

Time resolved photoluminescence was determined by using below band gap excitation (380 nm) source. The sample was measured at liquid He temperature. The transients are fitted by equation (5.35) as shown in figure 5.48. The lifetime is found to be 292 μs which is higher compared to in Mg-doped GaN:Eu.

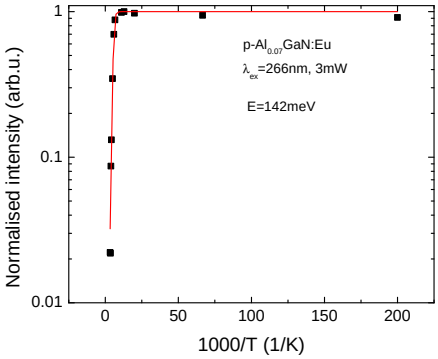

Figure 5.46: Arrhenius fitting of temperature dependent Eu^{3+} intensity in ALGaN:Eu

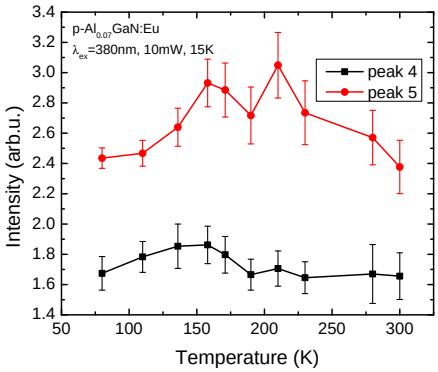

Figure 5.47: Temperature dependent Eu^{3+} photoluminescence intensity in AlGaN:Eu under below band gap excitation (380 nm)

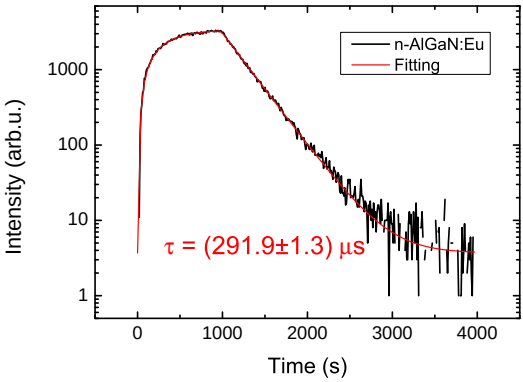

Figure 5.48: Photoluminescence lifetime of Eu^{3+} luminescence in AlGaN:Eu at liquid helium temperature.

5.4 General discussion about above results

The luminescence intensity of Eu^{3+} in Mg-doped GaN:Eu is enhanced than in u-GaN:Eu. Several optically active centers contributing to the Eu^{3+} luminescence have been observed. However, both Mg and Si doped GaN:Eu samples show most intense Eu^{3+} luminescence. The excitation of Eu^{3+}ion is based on donor-acceptor pair related energy transfer mechanism. In AlGaN host Eu^{3+} luminescence peaks found to have different intensity ratios and changed peak positions due to changes in the crystal field.

5.5 Other RE and transition metals in Nitrides

As the goal was to fabricate a single photon source, it is necessary to investigate luminescence from various rare earth ions such as cerium (Ce), erbium (Er) and various transition metals such as chromium (Cr), cobalt (Co) and nickel (Ni) in nitride host. In figure 5.49 the photo-luminescence spectra of Ce, Er and Eu in AlGaN host are shown. From the figure Eu^{3+} luminescence is clearly visible as small peaks around at 620 nm. However a broad peak at around 540 nm was observed for all the samples. In the literature it is reported that erbium has emission at 532 nm [34] and cerium has a broad luminescence band at 560 nm [20]. It is clear that erbium doped AlGaN does not show any erbium related visible luminescence. On the other hand cerium doped AlGaN show a broad band near the expected range. However, as all the implanted samples are showing the same emission peak it is very difficult to distinguish the real cerium emission rather, it is intended to say that the emission from all the samples related to some defects induced due to implantation.

In this case it is difficult to distinguish between the rare earth luminescence and defect luminescence. In figure 5.50 the photoluminescence spectra of Cr doped AlGaN and AlN

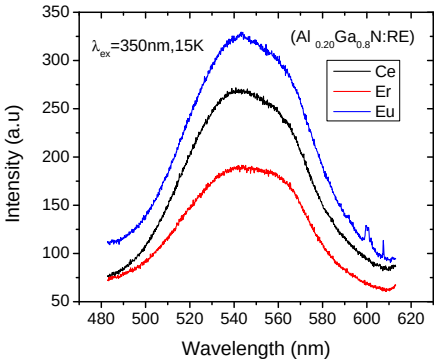

Figure 5.49: Photoluminescence spectra of cerium, erbium, and europium doped AlGaN at 15 K for λ_{ex}=350 nm excitation

at 15 K under 335 nm excitation is shown. Emission at 694 nm was expected from these samples [40]. Unfortunately there is no emission found related in this range. Similarly cobalt implanted GaN was investigated. Photoluminescence spectra at 15 K is shown in figure 5.51. Co related luminescence is expected at 662 nm [44]. However, from the figure 5.51 it is evident that no luminescence is observed related to cobalt. Smaller peaks in the spectrum might be related to host materials because the spectrum is not only observed in the implanted region but also in the nonimplanted region as well.

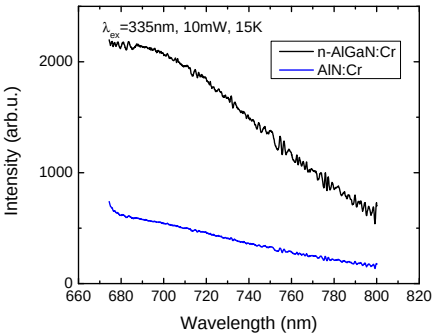

Figure 5.50: Photoluminescence spectra of Cr implanted nitrides at 15 K for λ_{ex}=335 nm excitation

As shown in figure 5.52 nickel doped GaN, AlGaN and AlN was investigated. Nickel related emission is expected at 503 nm [48]. However, any nickel related emissions was not observed. These peaks could be due to the substrate and present in whole region of the samples irrespective of implantation.

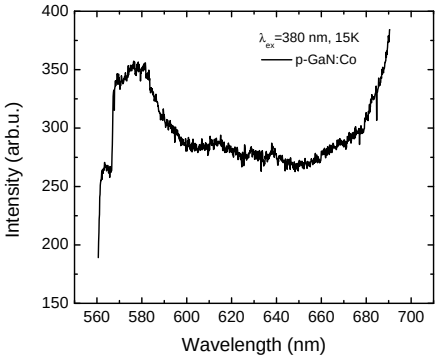

Figure 5.51: Photoluminescence spectra of cobalt implanted GaN at 15 K for λ_{ex}=380 nm excitation

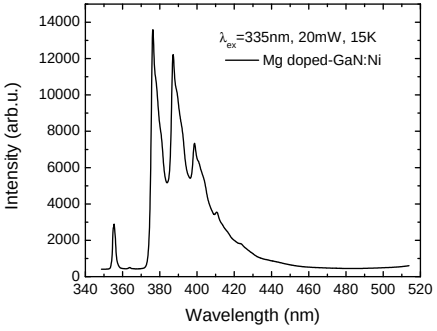

Figure 5.52: Photoluminescence spectra of Ni implanted Mg doped GaN at 15 K for λ_{ex}=335 nm excitation

6 Summary and Conclusions

In conclusion, Eu^{3+} luminescence in europium implanted various nitride hosts (u-GaN, p-GaN, AlGaN and AlN) is investigated and two different optical active centers (type I and type III) in Eu implanted Mg-doped GaN along with several other possible optical centers have been observed. The peaks belongs to two optical centers are identified. In contrast there are only one optical centers (type I) present in Eu implanted undoped GaN. The intensity of peaks belongs to type III center is found to be temperature independent. The excitation process is modeled by a resonant energy transfer from donor-acceptor pairs to the europium ions. From temperature dependent Eu^{3+} luminescence two activation energies are found under above band gap excitation. Under below band gap excitation the Eu^{3+} luminescence intensity remains constant and found no intrinsic nonradiative energy back transfer takes place from excited europium ions to the GaN host. This is also evident from the weak temperature dependence of the Eu^{3+} luminescence lifetime.

Moreover, in europium implanted GaN codoped with both Mg and Si we have found strong enhancement of Eu^{3+} luminescence which is essential for fabricating greater efficient red light emitting diode. Energy transfer to the europium ion is found to take place through the donor-acceptor pair.

In AlGaN:Eu we have found changes in Eu^{3+} luminescence peak positions and spectral

shape due to change in the crystal field.

Bibliography

[1] J. H. Park and A. J. Steckl, *Laser action in Eu-doped GaN thin-film cavity at room temperature*, Appl. Phys. Lett. **85**, 4588 (2004).

[2] A. Nishikawa, T. Kawasaki, N. Furukawa, Y. Terai, and Y. Fujiwara, *Room-Temperature Red Emission from a p-Type/Europium-Doped/n-Type Gallium Nitride Light-Emitting Diode under Current Injection*, Appl. Phys. Express **2**, 071004 (2009).

[3] R. Dahal, C. Ugolini, J. Y. Lin, H. X. Jiang, and J. M. Zavada, *Current-injected 1.54 μm light emitting diodes based on erbium-doped GaN*, Appl. Phys. Lett. **93**, 033502 (2008).

[4] J. Sawahata, H. Bang, J. Seo, K. Akimoto, *Optical processes of red emission from Eu doped GaN* Science and Technology of Advanced Materials **6**, 644, (2005).

[5] H. J. Lozykowski, W. M. Jadwisienczak, J. Han, and I. G. Brown, *Luminescence properties of GaN and Al0.14Ga0.86N/GaN superlattice doped with europium*, Appl. Phys. Lett. **77**, 767 (2000).

[6] A. Nishikawa, N. Furukawa, T. Kawasaki, Y. Terai, and Y. Fujiwara, *Improved luminescence properties of Eu-doped GaN light-emitting diodes grown by atmospheric-pressure organometallic vapor phase epitaxy*, Appl. Phys. Lett. **97**, 051113 (2010).

[7] D gun Lee, A. Nishikawa, Y. Terai, and Y. Fujiwara, *Eu luminescence center created by Mg codoping in Eu-doped GaN*, Appl. Phys. Lett. **100**, 171904 (2012).

[8] S. Kim, S. J. Rhee, X. Li, J. J. Coleman, and S. G. Bishop, *Selective enhancement of 1540 nm Er3+ emission centers in Er-implanted GaN by Mg codoping*, Appl. Phys. Lett. **76**, 2403 (2000).

[9] R. Wang, A. J. Steckl, E. E. Brown, U. Hömmerich, and J. M. Zavada, *Effect of Si codoping on Eu3+ luminescence in GaN*, J. Appl. Phys. **105**, 043107 (2009).

[10] Y. Takagi, T. Suwa, H. Sekiguchi, H. Okada and A. Wakahara, *Effect of Mg codoping on Eu3+ luminescence in GaN grown by ammonia molecular beam epitaxy*, Appl. Phys. Lett. **99**, 171905 (2011).

[11] K. Wang, R. W. Martin, K. P. O'Donnell, V. Katchkanov, E. Nogales, K. Lorenz, E. Alves, S. Ruffenach, and O. Briot, *Selectively excited photoluminescence from Eu-implanted GaN*, Appl. Phys. Lett. **87**, 112107 (2005).

[12] L. Bodiou, A. Oussif, A. Braud, J.-L. Doualan, R. Moncorgé, K. Lorenz, and E. Alves, *Effect of annealing temperature on luminescence in Eu implanted GaN* Opt. Mater. **28**, 780 (2006).

[13] Masanori Tanaka, Shinichi Morishima, Hyungjin Bang, Jeung Sun Ahn, Takashi Sekiguchi, Katsuhiro Akimoto, *Low-energy charge-transfer state and optical properties of Eu^{3+}-doped GaN* Phys. Status Solidi C **0**, 2639 (2003).

[14] Shinya Higuchi, Atsushi Ishizumi, Junji Sawahata, Katsuhiro Akimoto, and Yoshihiko Kanemitsu, *Luminescence and energy-transfer mechanisms in Eu^{3+}-doped GaN epitaxial films* Phys. Rev. B **81**, 035207 (2010).

[15] S.J. Chang, Y.C. Lin, Y.K. Su, C.S. Chang, T.C. Wen, S.C. Shei, J.C. Ke, C.W. Kuo, S.C. Chen, C.H. Liu, *Nitride-based LEDs fabricated on patterned sapphire substrates*, Solid-State Electronics, **47**, 1539, (2003).

[16] T. C. Wen, S. J. Chang, Y. K. Su, L. W. Wu, C. H. Kuo, W. C. Lai, J. K. Sheu, T. Y. Tsai, *InGaN/GaN multiple quantum well green light-emitting diodes prepared by temperature ramping*, J. Electron. Mater. **32**, 419 (2003).

[17] S. Nakamura, M. Senoh , N. Iwasa and S. Nagahama, *High-Brightness InGaN Blue, Green and Yellow Light-Emitting Diodes with Quantum Well Structures*, Japanese J. Appl. Phys. **34**, 797 (1995).

[18] J. Hader, J. V. Moloney, and S. W. Koch, *Temperature-dependence of the internal efficiency droop in GaN-based diodes* Appl. Phys. Lett. **99**, 181127 (2011).

[19] Zhiqiang Liu, Tongbo Wei, Enqing Guo, Xiaoyan Yi, Liancheng Wang, Junxi Wang, Guohong Wang, Yi Shi, Ian Ferguson, and Jinmin Li, *Efficiency droop in InGaN/GaN multiple-quantum-well blue light-emitting diodes grown on free-standing GaN substrate* Appl. Phys. Lett. **99**, 091104 (2011).

[20] S. R. Rotman and C. Warde, *Defect luminescence in cerium-doped yttrium aluminum garnet*, J. Appl. Phys. **58**, 522 (1985).

[21] A. Majid and A. Ali, *Red shift of near band edge emission in cerium implanted GaN*, J. Phys. D: Appl. Phys. **42** 045412 (2009).

[22] R. Xie, N. Hirosaki, M. Mitomo, Y. Yamamoto, T. Suehiro, N. Ohashi, *Photoluminescence of Cerium-Doped a-SiAlON Materials*, Journal of the American Ceramic Society **87**, 1368 (2004).

[23] Y. S. Lin, R. S. Liu, and B. M. Cheng, *Investigation of the Luminescent Properties of Tb3+-Substituted YAG:Ce, Gd Phosphors*, J. Electrochem. Soc. **152**, J41 (2005).

[24] D. Haranath, H. Chander, P. Sharma, and S. Singh, *Enhanced luminescence of Y3Al5O12:Ce3+ nanophosphor for white light-emitting diodes*, Appl. Phys. Lett. **89**, 173118 (2006).

[25] R. A. Hansel, S. W. Allison, and D. G. Walker, *Temperature-dependent luminescence of Ce3+ in gallium-substituted garnets*, Appl. Phys. Lett. **95**, 114102 (2009).

[26] G. Dieke and H. Crosswhite Appl. opt. **2**, 675 (1963).

[27] C. Lu, , W. Hsu, C. Huang, S.V. Godbole, B. Cheng, *Luminescence characteristics of europium-ion doped $BaMgAl_10O_17$ phosphors prepared via a solâ€“gel route employing polymerizing agents*, Mater. Chem. Phys. **90**, 62 (2005).

[28] X. Zhang, J. Zhang, J. Huang, X. Tang, M. Gong, *Synthesis and luminescence of Eu^{2+} doped alkaline-earth apatites for application in white LED* J. Lumin. 130, 554 (2010).

[29] M. Sato, T. Tanaka, and M. Ohta, *Photostimulated Luminescence and Structural Characterization of Ba5(PO4)3Cl:Eu^{2+} Phosphors*, J. Electrochem. Soc. **141**, 7, 1851(1994).

[30] J. A. Capobianco, P.P. Proulx, N. Raspa, *Optical spectroscopy and crystal field analysis of Eu^{3+} in calcium tartrate tetrahydrate*, Chem. Phys. Lett. **161**, 151 (1989).

[31] B. M Angelov, *Comparative crystal-field analysis of Eu^{3+}: Y_2O_3*, J. Phys. C: Solid State Phys. **16**, L437 (1983).

[32] H. Bang, S. Morishima, Z. Li, K. Akimoto, M. Nomura, E. Yagi, *MBE growth of Eu-or Tb-doped GaN and its optical properties*, J. Cryst. Growth **237-239**, 1027 (2002).

[33] B. Zheng, J. Michel, F. Y. G. Ren, L. C. Kimerling, D. C. Jacobson, and J. M. Poate, *Room-temperature sharp line electroluminescence at lambda =1.54 μm from an erbium-doped, silicon light-emitting diode*, Appl. Phys. Lett. **64**, 2842 (1994).

[34] U. Hömmerich, J.T. Seo, C.R. Abernathy, A.J. Steckl, J.M. Zavada, *Spectroscopic studies of the visible and infrared luminescence from Er doped GaN*, Materials Science and Engineering B **81**, 116 (2001).

[35] T. J. Kippenberg, J. Kalkman, A. Polman and K. J. Vahala, *Demonstration of an erbium-doped microdisk laser on a silicon chip*, Phys. Rev. A **74**, 051802(R) (2006).

[36] J. Palm, F. Gan, B. Zheng, J. Michel, and L. C. Kimerling , *Electroluminescence of erbium doped silicon*, Phys. Rev. B **54**, 17603 (1996).

[37] D. T. X. Thao, C. A. J. Ammerlaan, and T. Gregorkiewicz, *Photoluminescence of erbium-doped silicon: Excitation power and temperature dependence*, J. Appl. Phys. **88**, 1443 (2000).

[38] L. C. Cossolino and A. R. Zanatta, *Influence of chromium concentration on the optical electronic properties of ruby microstructures*, J. Phys. D: Appl. Phys. **43**, 015302 (2010).

[39] Y. Ahn, J. Seo, J. Park, *Diffusion of chromium in sapphire: The effects of electron beam irradiation*, J. Cryst. Growth **326**, 45 (2011).

[40] M. Soukieh, B.A. Ghani, M. hammadi, *Numerical calculations of intracavity dye Q-switched ruby laser* Opt. Lasers Eng. **41**, 177 (2004).

[41] T. H. Maiman, *Stimulated Optical Radiation in Ruby*, Nature **187**, 493 (1960).

[42] M. Maqbool, E. Wilson, J. Clark, I. Ahmad, and A. Kayani, *Luminescence from Cr+3-doped AlN films deposited on optical fiber and silicon substrates for use as waveguides and laser cavities*, Appl. Opt. **49**, 653 (2010).

[43] A. Ney, V. Ney, S. Ye, K. Ollefs, and T. Kammermeier, *Magnetism of Co doped ZnO with Al codoping: Carrier-induced mechanisms versus extrinsic origins*, Phys. Rev. B **82**, 041202 (2010).

[44] T. T. Loan, N. N. Long and L. H. Ha, *Photoluminescence properties of Co-doped ZnO nanorods synthesized by hydrothermal method*, J. Phys. D: Appl. Phys. **42** , 065412 (2009).

[45] W. K. Park, R. J. Ortega-Hertogs, J. S. Moodera, A. Punnoose, and M. S. Seehra, *Semiconducting and ferromagnetic behavior of sputtered Co-doped TiO2 thin films above room temperature*, J. Appl. Phys. **91**, 8093 (2002).

[46] D. Hou, R. Zhaoa, Y. Wei, C. Zhen, C. Pan, G. Tang, *Room temperature ferromagnetism in Ni-doped ZnO films*, Current Applied Physics **10**, 124, (2010).

[47] Z.G. Yin, N. Chen, F. Yang, S.L. Song, C.L. Chai, J. Zhong, H.J. Qian, K. Ibrahim, *Structural, magnetic properties and photoemission study of Ni-doped ZnO*, Solid State Commun. **135**, 430 (2005).

[48] S. M. Taheri and M. H. YousefiTuning, *luminescence of 3d transition-metal doped quantum particles: Ni+2: CdS and Fe+3: CdS*, Braz. J. Phys. **40**, 301 (2010).

[49] S. Fischer, C. Wetzel, E. E. Haller, and B. K. Meyer, *On p-type doping in GaN—acceptor binding energies*, Appl. Phys. Lett. **67**, 1298 (1995).

[50] Annamraju Kasi Viswanath, Joo In Lee, Sungkyu Yu, Dongho Kim, Yoonho Choi, and Chang-hee Hong, *Photoluminescence studies of excitonic transitions in GaN epitaxial layers*, J. Appl. Phys. **84**, 3848 (1998).

[51] L. S. Wang, W. K. Fong, C. Surya, K.W. Cheah, W.H. Zheng, Z.G. Wang, *photoluminescence of rapid thermal annealed Mg doped GaN films*, Solid-State Electronics **45**, 1153 (2001).

[52] U. Kaufmann, M. Kunzer, M. Maiser, H. Obloh, A. Ramakrishnan, B. Santic, P. Schlotter, *Nature of the 2.8 eV photoluminescence band in Mg doped GaN*, Appl. Phys. Lett. **72** ,1326 (1998).

[53] M. Lachab, D.-H. Youn, R.S. Qhalid Fareed, T. Wang, S. Sakai, *Characterization of Mg-doped GaN grown by metalorganic chemical vapor deposition*, Solid-State Electronics **44**, 1669 (2000).

[54] S. Kim, S. J. Rhee, X. Li, J. J. Coleman, and S. G. Bishop, *Selective enhancement of 1540 nm Er3+ emission centers in Er-implanted GaN by Mg codoping*, Appl. Phys. Lett. **76**, 2403 (2000).

[55] E. F. Schubert, I. D. Goepfert, W. Grieshaber, and J. M. Redwing, *Optical properties of Si-doped GaN*, Appl. Phys. Lett. **71**, 921 (1997).

[56] J. I. Pankove and J. A. Hutchby, *Photoluminescence of ion-implanted GaN* J. Appl. Phys. **47**, 5387 (1976).

[57] D. M. Hofmann, D. Kovaler, G. Steude, B. K. Meyer, A. Hoffmann, L. Eckey, R. Hertz, T. Detchprom, H. Amano, and I. Akasaki, *Properties of the yellow luminescence in undoped GaN epitaxial layers*, Phys. Rev. B **52**, 16 702 (1995).

[58] Spectra of Atoms and Molecules By Peter F. Bernath

[59] Thesis of Jia Guohua, *Spectroscopy and energy transfer in metal ion doped oxides*, University of Hongkong

[60] Atomic and Molecular Spectra physics by rajkumar

[61] Quantum chemistry By Donald Allan McQuarrie

[62] B.R. Judd, *Optical Absorption Intensities of Rare-Earth Ions*, Phys. Rev. **127**, p. 750 (1962).

[63] G. S. Ofelt, *Intensities of Crystal Spectra of Rare-Earth Ions*, J. Chem. Phys. **37**, p. 511 (1962).

[64] Q. Xiao, Y. Liu, L. Liu, R. Li, W. Luo, and X. Chen, *Eu3+ Doped In2O3 Nanophosphors: Electronic Structure and Optical Characterization*, J. Phys. Chem. **114**, p. 9314 (2010).

[65] Jorma Hölsä, Markku Leskelä, *Fluorescence spectrum, energy level scheme and crystal field analysis of europium(+III) doped lanthanum magnesium borate LaMgB5O10:Eu3+*, Molecular physics **54**, p. 675 (1985).

[66] J. A. Capobianco, P.P. Proulx and N. Raspa, *Optical spectroscopy and crystal field of* Eu^3+ *in calcium tartrate tetrahydrate*, Chem. Phys. Lett. **161**, p. 151 (1989).

[67] Spectroscopy of Solid-state Laser and Luminescent Materials by Zundu Luo *etal.*

[68] K Binnemans, C. Görller-Walrand, *Application of the Eu3+ ion for site symmetry determination*, Journal of rare earth **14**, p. 173 (1996).

[69] J. D. Dunitz, P. Hemmerich, R. H. Holm, J. A. Ibers, C. K.Jorgensen, J. B. Neilands, D.Reinen, and R. J. P. Williams, *Structure and Bonding*, Springer **22** (1975).

[70] John B. Gruber, Ulrich Vetter, Takashi Taniguchi, Gary W. Burdick, Hans Hofsass, Sreerenjini Chandra, and Dhiraj K. Sardar, *Spectroscopic analysis of Eu 3+ in single-crystal hexagonal phase AlN*, J. Appl. Phys. **110**, p. 023104 (2011).

[71] J. Han Kim and P. H. Holloway, *Room-temperature photoluminescence and electroluminescence properties of sputter-grown gallium nitride doped with europium*, J. Appl.Phys, **95**, p. 4787 (2004).

[72] A. J. Steckl, J. C. Heikenfeld, D. S. Lee, M. J. Garter, C. C. Baker, Y. Q.Wang, and R. Jones, *Rare-Earth-Doped GaN: Growth, Properties, and Fabrication of Electroluminescent Devices* IEEE J. Sel. Top. Quantum Electron. **8**, p. 749 (2002).

[73] H. Peng, C. Lee, H. O. Everitt, C. Munasinghe, D. S. Lee, *Spectroscopic and energy transfer studies of Eu3+ centers in GaN*, J. Appl. Phys. **102**, p. 073520 (2007).

[74] K. P. O'Donnell and B. Hourahine, *Rare earth doped III-nitrides for optoelectronics*, Eur. Phys. J. Appl. Phys. **36**, p. 91 (2006).

[75] K. P. O'Donnell, V. Katchkanov, K. Wang, R.W. Martin, P.R. Edwards, B. Hourahine, E. Nogales, J.F.W. Mosselmans, B. De Vries, and the RENiBEl Consortium*Site multiplicity of rare earth ions in III-nitrides*, Mater. Res. Soc. Symp. Proc. **831** p. 527 (2005).

[76] Simone Sanna, W. G. Schmidt, Th. Frauenheim, and U. Gerstmann, *Rare-earth defect pairs in GaN: LDA+U calculations*, Phys. Rev. B **80**, p. 104120 (2009).

[77] Z. Fleischman, C. Munasinghe, A. J. Steckl, A. Wakahara, J. Zavada and V. Dierolf, *Excitation pathways and efficiency of Eu ions in GaN by site-selective spectroscopy*, Appl. Phys. B **97**, p. 607 (2009).

[78] H. J. Lozykowski, *Kinetics of luminescence of isoelectronic rare-earth ions in III-V semiconductors*, physicsal review B **48**, p. 17758 (1993).

[79] C. S. Zhang, H. B Xiao, Y. J. Wang, Z. J. Chen, X. L. Cheng, and F. Zhang, J. Mater. Res.,*Thermal quenching behavior of Er-doped silicon-rich SiO2 prepared by ion implantation*, J. Mater. Res. **19**, p. 2699 (2004).

[80] J. Michel, J. L. Benton, R.F. Ferrante, D.C. Jacobson, D.J. Eaglesham, E.A. Fitzgerald, Y.H. Xie, J.M. Poate, and L.C. Kimerling, *Impurity enhancement of the 1.54μm Er3+ luminescence in silicon*, J. appl. phys. **70**, p. 2672 (1991).

[81] M. M. Mezdrogina, E. Yu. Danilovskii, and R. V. KuzÓin, *Emission from Rare Earth Ions in GaN Wurtzite Crystals*, Inorganic Materials **47**, p. 1450 (2011).

[82] D. G. Thomas, and J. J. Hopfield, *Isoelectronic Traps due to Nitrogen in Gallium Phosphide*, Phys. Rev. **150**, pp. 680 (1966).

[83] J. W. Allen, *Isoelectronic Impurities in Semiconductors: a Survey of Binding Mechanisms*, J. Phys. C, vol. **4**, p 1936 (1971).

[84] P. Dorenbos and E. van der Kolk, *Location of lanthanide impurity levels in the III-V semiconductor GaN*, Appl. phys. lett. **89**, p. 061122 (2006).

[85] T. Hoshina, S. Imanaga, and S. Yokono, *Charge transfer effects on the luminescent properties of* Eu^{3+}, J. Lumin **15**, p. 455 (1977).

[86] J. F. Ziegler, www.srim.org (2008 version)

[87] Jia Guohua, dissertation, *Spectroscopy and energy transfer in metal ion doped complexes*, city university Hongkong, (2009).

[88] I. S. Roqan, K. P. ODonnell, R. W. Martin, P. R. Edwards, S. F. Song, A. Vantomme, K. Lorenz, E. Alves, and M. Bockowski, *Identification of the prime optical center in GaN:*Eu^{3+} Phys. Rev.B **81**, 085209 (2010).

[89] Z. Fleischman, C. Munasinghe, A. Steckl, A. Wakahara, J. Zavada, and V. Dierolf, *Excitation pathways and efficiency of Eu ions in GaN by site-selective spectroscopy*, Appl. Phys. B **97**, 607 (2009).

[90] S. Chang-Sik, K. Seong-II, K. Young-Hwan, K. Y. Tae, C. In-Hoon, A. Wakahara, H. Tanoue, M Ogura, *Red Emission from Eu-Implanted GaN*, J. Korean Phys. Soc. **45**, S519, (2004).

[91] N. Woodward, J. Poplawsky, B. Mitchell, A. Nishikawa, Y. Fujiwara, and V. Dierolf *Excitation of Eu^{3+} in gallium nitride epitaxial layers: Majority versus trap defect center* Appl. Phys. Lett. **98**, 011102 (2011).

[92] W. Badalawa, H. Matsui, T. Osone, N. Hasuike, H. Harima, and H. Tabata, *Correlation between structural and luminescent properties of Eu^{3+}-doped ZnO epitaxial layers* J. Appl. Phys. **109**, 053502, (2011).

[93] K. Wang, K. P. O'Donnell, B. Hourahine, R. W. Martin, I. M. Watson, K. Lorenz, and E. Alves *Luminescence of Eu ions in AlxGa1-xN across the entire alloy composition range*, Phys. Rev. B **80**, 125206 (2009).

Acknowledgement

Finally, I would like to take the opportunity to make a big thank you to those who have contributed directly or indirectly to the success of this work:

- First of all I would like to give a hearty thanks to Prof Hangleiter who has given me the opportunity to pursue my research in his group and I would be grateful to him for his support and meaningful discussions during my work.

- My further thanks to all current and former members of the working group, with all their cooperation: Torsten Langer, Ronald Buss, Andreas Kraus, Christopher Hein, Alexis Fedor, Ailun Zhao, Dr. Heiko Bremer, and Dr. Uwe Rossow.

  The former members of the working group: Holger Jönen, Lars Hoffmann, Moritz Brendel, Peter Clodius, Martina Thomsen and Daniel Dräger. I would also like to thank Dr. Fathi Gouider for his help in need.

- I would like to thank to Prof. Meinhard Schilling, and all members of IGSM for their great help in discussing and providing nice atmosphere for international students.

- For technical problems or management issues Diana Deuse, Frank Werner, Ingeborg Westphal and Dagmar Schumacher always a great help.

- For the pleasant working atmosphere I would like to thank all the staff of the Institute of Applied Physics.

I would like to give a special thank to my father who always motivated me for higher study and would have been the happiest person to see me here, had he been alive. Moreover, I would like to thank to all of my family members specially to my mother, my brother (*Kunanana*), my sisters (*Kuninani, Tuninani and Manjunani*) and my wife (*Jyotsna*) for all their support. Thanks to my friends *Narahari, Rajeeb, Rakshyakara, Napoleon and Bidya* for their mentally support during this period.

CV

Name:	Jayanta Kumar Mishra
Date of birth:	01 May 1981
Place of Birth:	Saharpada, Odisha, India
Marital status:	Married
Nationality:	Indian

1993 - 1995	High School at Saharpada high school, Odisha, India
1995 - 1997	Intermediate at karanjia college, Odisha, India
1997 - 2000	Bachelor of Science, at North Orissa university, Odisha, India
2000 - 2002	Master of Science in Physics at North Orissa university, Odisha, India
2005 - 2007	Master of Technology in material science and engineering at I.I.T. Kharagpur, India
2008 - 2013	Research fellow at Institut für Angewandte Physik, TU Braunschweig